Acta Astronautica 217 (2024) 145–161

Contents lists available at ScienceDirect

Acta Astronautica

journal homepage: www.elsevier.com/locate/actaastro

A constellation design for orbiting solar reflectors to enhance terrestrial solar energy☆

Onur Çelik *, Colin R. McInnes

Space and Exploration Technology Group, James Watt School of Engineering, University of Glasgow, Glasgow G12 8QQ, Scotland, United Kingdom

ARTICLE INFO

Keywords:
Space-based solar energy
Orbiting solar reflectors
Satellite constellations
Astrodynamics
Genetic optimisation

ABSTRACT

Orbiting solar reflectors (OSRs) are flat, thin and lightweight reflective structures that are proposed to enhance terrestrial solar energy generation by illuminating large terrestrial solar power plants locally around dawn/dusk and during night hours. The incorporation of OSRs into terrestrial energy systems may offset the daylight-only limitation of terrestrial solar energy. However, the quantity of solar energy delivered to the Earth's surface remains low due to short duration of orbital passes and the low density of the reflected solar power due to large slant ranges. To compensate for these, this paper proposes a constellation of multiple reflectors in low-Earth orbit for scalable enhancement of the quantity of energy delivered. Circular near-polar orbits of 1000 km altitude in the terminator region are considered in a Walker-type constellation for a preliminary analysis. Starting from a simplified approach, the equations of Walker constellations describing the distribution of the reflectors are first modified by introducing a phasing parameter to ensure repeating pass-geometry over solar power farms. This approach allows for a single groundtrack optimisation to define the constellation, which was carried out by a genetic algorithm for single and two reflectors per orbit with an objective function defined as the total quantity of energy delivered per day, to existing and hypothetical solar power projects around the Earth. When full-scale constellations are considered with a number of reflectors, the quantity of solar energy delivered is substantial in the broader context of global terrestrial solar energy generation.

1. Introduction

Orbiting solar reflectors are large, thin and ultra-lightweight reflector structures in orbit, proposed to illuminate the Earth for a variety of applications. The earliest proposals are before the modern space era and included the illumination of cities and locations such as airports at night [1]. The later proposals in the 1970s and 1980s extended those applications to terrestrial solar energy generation by illuminating ultra-large utility-scale solar power farms at night, enhancing agriculture and street illumination [2–4]. Global demand for clean energy due to climate change, decreasing launch costs due to commercialisation and other advancements in space technologies such as in-orbit assembly and manufacturing have attracted renewed interest in the concept of orbiting solar reflectors in the 21st century [5].

The most important limitation of terrestrial solar energy generation is its restriction to daylight hours, which, despite the Sun as a practically endless source of energy, limits the electricity generation from solar power farms to a much lower level than their actual capacity. To that end, a reflector in orbit, placed in orbits that are both visible to the Sun and to the solar power farm, could extend the operational hours by illuminating the farm locally, thereby enhancing its utility [5]. The concept of orbiting solar reflectors has therefore been studied for the 21st century energy demands and requirements by leveraging the advancements in space technology. Fraas and co-authors have studied this concept primarily for the enhancement of solar energy [6–9] but also for municipal street lighting [10]. Among more recent studies, Bonetti & McInnes presented a two-reflector constellation in a so-called anti-heliotropic orbit to deliver solar energy to three ultra-large hypothetical solar power farms in equatorial regions [11]. Viale et al. instead presented a reference architecture study for near-term applications with a five-reflector system in Sun-synchronous orbits, delivering solar energy to 13 existing and under-development solar power farms around the Earth [12]. The authors also presented a technology roadmap for the employment of the concept of orbiting solar reflectors [13]. Other proposals of OSRs include a dual reflector system with a Sun-facing parabolic reflector and a small, agile and steerable reflector in orbits displaced on either side of the terminator line to further enhance the

☆ This manuscript is based on the manuscript presented at International Astronautical Congress, 74, Baku, Azerbaijan, 2–6 October 2023. Paper no. IAC-23,C1,IPB,4,x77299. Copyright by the authors.

* Corresponding author.
E-mail addresses: Onur.Celik@glasgow.ac.uk (O. Çelik), Colin.McInnes@glasgow.ac.uk (C.R. McInnes).

https://doi.org/10.1016/j.actaastro.2024.01.031
Received 28 November 2023; Received in revised form 24 January 2024; Accepted 25 January 2024
Available online 30 January 2024
0094-5765/© 2024 The Authors. Published by Elsevier Ltd on behalf of IAA. This is an open access article under the CC BY license (http://creativecommons.org/licenses/by/4.0/).

energy delivery [14]. Orbiting solar reflectors are also considered in lieu of battery technology for terrestrial solar energy [15].

The quantity of energy delivered from orbiting solar reflectors is scalable by the number and size of the reflectors [13,16]. Single reflectors may be increased in size to enhance the quantity of solar energy delivered, which would increase solar power density on the ground but it would not extend the daily operational hours. Instead, a number of reflectors may be considered in a constellation that could provide continuous, scalable and predictable solar energy input to a solar power farm. Ehricke's (1979) Powersoletta constellations envisaged a very large number of reflectors in a constellation to provide electricity to the entire Earth by only solar energy [3]. On the other hand, Canady & Allen (1982) considered a four-reflector constellation to illuminate several major cities in the United States [4]. Frass (2012, 2013) constellations consisted of 18 satellites in a single dawn/dusk orbit at 1000 km altitude, servicing some 40 hypothetical solar power farms on its groundtrack [6,7]. Bonetti & McInnes (2019) employed a much larger altitude elliptical orbit and a flower constellation pattern [17] for a two-reflector constellation to deliver solar energy to hypothetical large equatorial solar power farms [11]. Viale et al. (2023) reference architecture study may also be considered a form of constellation with five reflectors in a closely spaced train motion in a single, 24-h repeating ground track dawn-dusk Sun-synchronous orbit, whose ground track is "anchored" to an existing solar power farm project [12]. However, none of these studies consider optimal constellations that consider solar power farms that are existing or under development with realistic models of solar energy delivery and provide detailed insights into individual passes.

Constellations of orbiting solar reflectors may need to satisfy several requirements. For a truly global solar energy delivery at dawn and dusk hours, orbits of near-polar inclinations placed at near-terminator regions are more desirable. Especially Sun-synchronous orbits provide natural Sun-tracking ability by exploiting the Earth's oblateness [5]. But widely used constellation geometries such as Walker constellation [18] and more generalised Flower constellations [17] distribute orbit planes around the Earth equally and not specific regions. Moreover, continuous and scalable energy delivery requires reflectors to be placed in orbits in such a way to follow the same pass geometry over solar power farms. This requires the distribution of orbit planes and the reflectors on them to be synchronised with the Earth's rotation in the presence of the Earth's oblateness, which may also be defined by a phase angle between them to be controllable. Arnas & Casanova (2020) tackles a similar problem by using the analytical expressions of Flower and Walker constellations, though they only consider constellations equally distributed globally and use time instead of a phase angle [19]. Considering the existing, under development and hypothetical farms with an objective to maximise the daily quantity of solar energy delivered globally, the constellation design problem becomes an optimisation problem of a new kind. The constellations with repeating pass geometries would, in fact, make this problem an optimisation problem of a single reflector's groundtrack where the distribution of others in the orbit plane and mean anomaly would provide the same pass geometry for a scalable expansion.

This paper therefore presents an optimal constellation design for orbiting solar reflectors to enhance terrestrial solar energy generation. A Walker constellation pattern is considered with polar and near-polar Sun-synchronous circular orbits at 1000 km altitude. First, starting from a simplified approach of multiple reflectors in a single orbit and non-rotating Earth, the scalability aspects are discussed in relation to the phase angle between reflectors. This phase angle is later used to modify the analytical distribution of reflectors in a Walker constellation pattern to synchronise successive orbit planes with Earth's rotation in the presence of Earth's oblateness perturbation to ensure the same pass geometry for all reflectors in the constellation. The groundtrack optimisation of the initial reflector satellite is then carried out by using a genetic algorithm with an objective function defined as the maximum daily energy delivery. The optimisation function includes a realistic model of reflected solar energy delivery [20]. A single-reflector and two-reflector configurations are considered in the optimisation by delivering solar energy to existing and hypothetical solar power farms. Detailed investigations of individual solutions are offered and discussed comparatively with other works. 5, 10 and 20-reflector constellations are presented and discussed in the wider context of enhancing terrestrial solar energy.

This paper is structured as follows: In the next section, the model for reflected solar energy delivery will be summarised. In Section 3, the approach for constellation design will be introduced. The optimisation problem will be discussed in Section 4 and the results of the optimisation will be discussed in Section 5. Section 6 will expand on the implications of the results for reflector constellation and, finally, conclusions will be presented in Section 7.

2. Reflected solar energy delivery from space

The power delivered by a reflector in orbit to the surface of the Earth can be written as follows [16]:

$$P_{SPF} = \chi(t) I_0 \frac{A_M}{A_{im}(t)} A_{SPF} \cos\frac{\psi(t)}{2} \tag{1}$$

where I_0 is the solar constant which is assumed to follow an inverse-square law with the distance from the Sun and equal to 1.37 GW km^{-2} at the mean distance between the Earth and the Sun, i.e. 1 Astronomical Unit (AU). A_M, A_{SPF}, A_{im} are the areas of the reflector, solar power farm and the projected image of the Sun (i.e., illuminated region) on the ground. A_M and A_{SPF} have fixed areas, but A_{im} is an elliptical area whose size is a time-dependent function that can be written as [20]:

$$A_{im}(t) = \pi a(t) b(t) = \pi \frac{[d(t)\tan(\alpha/2)]^2}{\sin\epsilon(t)} \tag{2}$$

where d denotes the magnitude of the slant range vector measured from the topocentric-horizon reference frame (THF) of the ground target such as a solar power farm and α denotes the angle subtended by the Sun, approximately 0.0093 rad at 1 AU. ϵ denotes the elevation angle measured from the local horizontal, defined again in the topocentric frame of the ground target and is given by [20]:

$$\epsilon(t) = \arcsin\frac{z_{THF}(t)}{d(t)} \tag{3}$$

where z_{THF} is the z-axis component of the slant range vector and given in Ref. [20]. The details of the derivation of Eqs. (2) and (3) will not be provided in this paper for conciseness, but in a recent paper Çelik & McInnes presented detailed analytical derivations as a function of orbital elements for both as a three-dimensional vector model by including the Earth's rotation and the Earth's oblateness perturbation for applications to Sun-synchronous orbits [20]. A simplified scalar model is also presented for polar orbits in Çelik & McInnes [16].

Of the other terms in Eq. (1), the time-dependent atmospheric transmission efficiency, $\chi(t)$ is provided with the following empirical relationship [21]:

$$\chi(t) = 0.1283 + 0.7559 e^{-0.3878\sec(\pi/2-\epsilon(t))} \tag{4}$$

Finally, $\psi(t)$ is the incidence angle, measured as the angle between the incoming and outgoing sunlight. $\psi(t)$ is also a time-dependent function where the incoming sunlight is dependent on the Sun vector and the outgoing sunlight is dependent on the reflector's position with respect to the solar power farm. A perfect pointing for the reflector is assumed as the effect of pointing errors in the quantity of energy delivered is considered minimal with an appropriate attitude control system design [22].

Therefore, the quantity of the energy delivered, E to the surface can be calculated by integrating Eq. (1) over a desired duration, such that:

$$E = \int_0^t P_{SPF} \mathrm{d}\tau \tag{5}$$

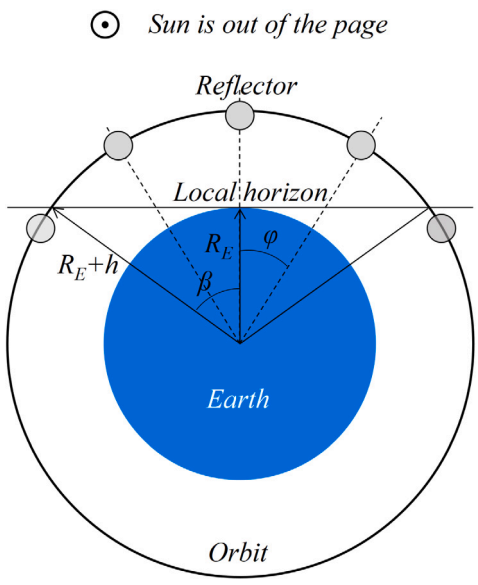

Fig. 1. Schematics of a simplified constellation design approach with multiple satellites in one orbit around a non-rotating Earth.

where t is time. t is typically the pass duration over a solar power farm, T_{pass}. In the three-dimensional reflected solar energy delivery model presented by Çelik & McInnes, T_{pass} is found by generating the z_{THF} and d profiles semi-analytically in the topocentric frame of a given solar power farm for a given time span and finding the time points where ϵ becomes 0 deg and 180 deg, where the difference between them is equal to T_{pass} [20]. In more simplified approaches where the Earth is non-rotating, T_{pass} can be found in a more straightforward way by finding the cone angle, measured as the angle between the Earth and orbit radii vectors extending from the centre of the Earth to the point where the local horizontal plane of the solar farm intersects with the orbit. This approach will first be used in the preliminary design of the constellations presented next.

3. Constellation design

3.1. Simplified approach

The simplified approach aims to provide an understaning of how the geometry of the constellation reflectors affects the reflected sunlight delivery. For this preliminary analysis, it is assumed that the Earth is non-rotating and the reflectors are separated by a phase angle ϕ in one orbit, as shown in Fig. 1.

According to Fig. 1, the cone angle defines the angle between the line that extends from the Earth's centre to the solar power farm and the line that extends from the Earth's centre to the intersection point of the orbit and the local horizontal plane can be expressed as:

$$\beta = \arccos \frac{R_E}{R_E + h} \tag{6}$$

According to this, the maximum number of reflectors in view can be written as:

$$N_{view}^{max} = \texttt{ceil}\left(\frac{2\beta}{\phi}\right) \tag{7}$$

where `ceil()` denotes the ceiling function that outputs the nearest equal or greater integer value. The next reflector satellite would appear in view after some time t_{n+1} that can be expressed as:

$$t_{n+1} = \frac{\phi}{\omega_o} \tag{8}$$

where ω_o is the orbit angular speed, defined as $\omega_o = \frac{2\pi}{T}$ with T denoted as orbit period:

$$T = 2\pi\sqrt{\frac{(R_E + h)^3}{\mu}} \tag{9}$$

with μ as the gravitational parameter, i.e., $\mu = 398\,600$ km^3 s^{-2}.

If there is more than one satellite separated by a phase angle ϕ, the pass duration, T_{pass}, can be extended by some ΔT_{ext}:

$$\Delta T_{ext} = \frac{T_{pass}\phi}{2\beta} = \beta\frac{T}{\pi}\frac{\phi}{2\beta} = \frac{T\phi}{2\pi} \tag{10}$$

The reflected sunlight from successive reflectors would also overlap for a duration T_{over}:

$$T_{over} = \frac{T_{pass}(\beta - \phi)}{\beta} = \beta\frac{T}{\pi}\frac{(\beta - \phi)}{\beta} = \frac{T(\beta - \phi)}{\pi} \tag{11}$$

As the Earth is assumed non-rotating and the reflector spacecraft are in the same orbit, their pass geometry and energy delivery properties would in principle be the same, such that the quantity of total energy delivered by a single reflector can be linearly scaled with the number of reflectors as:

$$E_{tot} = NE \tag{12}$$

where E_{tot} is the total quantity of energy delivered, N is the number of reflectors and E is the quantity of energy delivered by a reflector. This scalability offers the advantage of analysing the problem with a few parameters and for a single satellite but it is evidently oversimplified. Generalising this to a more realistic case with the Earth rotation will require a more detailed constellation analysis, which is tackled in the next subsection.

3.2. Repeating pass geometries with modified walker constellations

The basic idea presented in the previous section will be generalised to a more realistic case of rotating Earth, which would mean that the reflector spacecraft will no longer be in the same orbit but in separate orbit planes, arranged such that the pass geometry of each spacecraft is the same. To analyse the details of the problem, first Walker constellations will be considered [18]. Walker constellations are one of the most common orbit constellations [18], widely used for applications such as navigation [23]. The satellites in Walker constellations would possess the same orbit radius, eccentricity and inclination, and would be distributed in the right ascension of the ascending node (RAAN) and mean anomaly space equally for a given number of orbits and satellites and a phasing parameter [18]. The state-space form of this distribution can be expressed as follows [18]:

$$\begin{bmatrix} N_o & 0 \\ N_p & N_{so} \end{bmatrix}\begin{bmatrix} \Omega_{mn} - \Omega_{11} \\ M_{mn} - M_{11} \end{bmatrix} = 2\pi\begin{bmatrix} m-1 \\ n-1 \end{bmatrix} \tag{13}$$

where N_o denotes the number of orbits, N_{so} denotes the number of satellites per orbit, N_p denotes a phasing parameter that takes integer values in the range $N_p \in [0\ N_o\text{-}1]$. Note that the phasing parameter N_p is different than the phase angle ϕ. Ω and M are RAAN and mean anomaly, respectively, and m and n are the indices of orbits and satellites, respectively. Ω and M can also be rewritten as [18]:

$$\Omega_{mn} = \Omega_{11} + \frac{2\pi}{N_o}(m-1) \tag{14a}$$

$$M_{mn} = M_{11} + \frac{2\pi}{N_{so}}(n-1) - \frac{N_p}{N_{so}}\Delta\Omega \tag{14b}$$

where $\Delta\Omega = \Omega_{mn} - \Omega_{11}$. The general form of the Walker constellation given in Eq. (14) distributes the orbit planes equally around the Earth by $2\pi/N_o$ term. On the one hand, this is not useful for orbiting solar reflector applications, as the primary aim is to deliver solar energy at dawn/dusk around the terminator region. On the other hand, it is also not clear what other angle can replace 2π in Eq. (14)a. As

the aim of the reflector constellations is to ensure the same geometry across all reflectors, the separation between the orbit planes will be set accordingly. If the Earth's rotation is taken into account, the subsequent reflector's orbit needs to be synchronised with this rotation to ensure the same geometry, such that:

$$\Delta\Omega = \omega_E t_{n+1} = \frac{\omega_E}{\omega_o}\phi \tag{15}$$

where ω_E is the Earth's rotation rate, $\omega_E = 7.272 \times 10^{-5}$ rad/s. However, if the Earth's oblateness is taken into account, the orbit plane of all reflectors will also precess due to this perturbation. In this paper, the Earth's oblateness up to the second order (i.e., $J_2 = 1082.63 \times 10^{-3}$) is considered, whose impact on RAAN can be expressed as the rate of change [24]:

$$\dot{\Omega}_{J_2} = -\frac{3}{2}J_2\left[\frac{\sqrt{\mu}R_E^2}{(R_E+h)^{7/2}}\right]\cos i \tag{16}$$

where i is the orbit inclination. Therefore, the precession in the orbit plane of the subsequent spacecraft by considering the J_2 effect can be expressed as:

$$\Delta\Omega_{J_2} = -\dot{\Omega}_{J_2} t_{n+1} = -\dot{\Omega}_{J_2}\frac{\phi}{\omega_o} \tag{17}$$

It is worth noting that the orbit angular rate will also be altered as a result of the Earth's oblateness, due to the change in the orbit period, which can be expressed as:

$$T_{J_2} = T\left[1 - \frac{3}{2}J_2\frac{R_E^2}{(R_E+h)^2} - \frac{3}{4}J_2\frac{\left(4-5\sin^2 i\right)R_E^2}{(R_E+h)^2}\right] \tag{18}$$

Finally, combining Eqs. (15) and (17) would yield the angular separation between orbit planes, such that:

$$\Delta\Omega = \left(\frac{\omega_E - \dot{\Omega}_{J_2}}{\omega_{o,J_2}}\right)\phi \tag{19}$$

where ω_{o,J_2} is the J_2 altered orbit angular rate and is equal to $\omega_{o,J_2} = 2\pi/T_{J_2}$. Then, if the 2π term at the right-hand side of Eq. (14)a is redefined as some angle η_Ω, it can be found as:

$$\eta_\Omega = \left(\frac{\omega_E - \dot{\Omega}_{J_2}}{\omega_{o,J_2}}\right)\phi N_o \tag{20}$$

If, for example, a constellation is considered with six orbit planes and $\phi = 15$ deg separation between them, η_Ω would become 6.58 deg in which the orbit planes would be equally distributed in this range.

In a case where the orbit is unperturbed, an initial shift in mean anomaly M by ϕ would ensure that subsequent reflectors would follow the same pass geometry. However, the Earth's oblateness also rotates the orbit itself (i.e., shifts the start/end point of the orbit), such that [24]:

$$\dot{\omega}_{J_2} = -\frac{3}{2}J_2\left[\frac{\sqrt{\mu}R_E^2}{(R_E+h)^{7/2}}\right]\left(\frac{5}{2}\sin^2 i - 2\right) \tag{21}$$

where ω denotes the argument of pericentre. Then the shift in ω can be described as:

$$\Delta\omega = -\dot{\omega}_{J_2} t_{n+1} = -\frac{\dot{\omega}_{J_2}}{\omega_{o,J_2}}\phi \tag{22}$$

$\Delta\omega$ can now be combined with the unperturbed mean anomaly shift $M - \phi$ and orbit plane separation $\Delta\Omega$ in Eq. (19) to describe the distribution of reflectors in a constellation of m orbit planes with a *single* reflector in each orbit:

$$\Omega_m = \Omega_{11} + \left(\frac{\omega_E - \dot{\Omega}_{J_2}}{\omega_{o,J_2}}\right)\phi(m-1) \tag{23a}$$

$$M_m = M_{11} - \left(1 + \frac{\dot{\omega}_{J_2}}{\omega_{o,J_2}}\right)\phi(m-1) \tag{23b}$$

Table 1
Some examples of the relationship between ϕ, $\Delta\Omega$, ΔM and extension of pass duration ΔT_{ext}.

ϕ [deg]	$\Delta\Omega$ [deg]	ΔM [deg]	ΔT_{ext} [min]
5	0.37	4.99	1.44
15	1.10	14.98	4.32
30	2.19	29.98	8.65

The parameter n is not in the set of equations as there is one reflector per orbit, which is due to the second term in the right-hand side of Eq. (14) becoming zero for a single reflector per orbit. Table 1 shows how the separation between orbit planes $\Delta\Omega$ and mean anomaly values ΔM, alongside associated pass duration extension from Eq. (10), for three different ϕ values.

The effect of the Earth's oblateness perturbation is relatively small but still needs to be added in order to account for their effect on the evolution of constellations. The values are approximately linearly scaled with the angular separation ϕ. Closely spaced constellations could extend the pass duration only for a few minutes but can be extended by increasing the separation between them. These aspects will be discussed further in the design of the reflector constellations.

Eq. (23)b can be expanded to include more satellites per orbit by including the same term in Eq. (14)b by replacing 2π term with some angle η_M for further customisation of the constellation:

$$\Omega_{mn} = \Omega_{11} + \left(\frac{\omega_E - \dot{\Omega}_{J_2}}{\omega_{o,J_2}}\right)\phi(m-1) \tag{24a}$$

$$M_{mn} = M_{11} + \frac{\eta_M}{N_{so}}(n-1) - \left(1 + \frac{\dot{\omega}_{J_2}}{\omega_{o,J_2}}\right)\phi(m-1) \tag{24b}$$

The description of the constellation orbits in Eqs. (23) and (24) ensures that the reflectors will exhibit the same pass geometry as they pass over a solar power farm. Even if there is more than one reflector per orbit, the second reflector in the subsequent orbit would also follow the same geometry as the second reflector in the previous orbit plane. This will be used to investigate dawn/dusk clusters of constellation reflectors later. To demonstrate the same pass geometry among all reflectors, a constellation of six reflectors in six orbit planes at 1000 km altitude is analysed to observe the elevation profile (in distance) from the local horizontal plane of a hypothetical equatorial solar power farm. The elevation profile is given in Fig. 2.

Fig. 2 already shows the closely spaced passes over the solar power farms that reach up to the same height. However, Fig. 2(b) in particular shows a close-up of passes that happen approximately after 12 h. The close-up figure shows how all six reflectors reach up to the same height, where the error between them is found to be at the sub-meter level, therefore it can be confirmed that the pass geometry will be the same for all reflector spacecraft. The advantage of the same pass geometry is that, it would be no longer necessary to consider all reflector satellites in all orbit planes in the constellation optimisation, but the first reflector's orbit. The orbits and mean anomaly values of the rest of the reflector satellites can then distributed according to Eqs. (23) and (24) and the result can be generalised. But care must still be taken to set the optimisation problem to ensure the range of orbits is appropriately placed in the terminator region to avoid conditions such as eclipses. This will be discussed next.

4. Groundtrack optimisation

The optimisation problem tackled in this paper incorporates the energy delivery process and the placement of the orbit in the orbital element space. A single 1000 km circular orbit is considered throughout, but both polar and Sun-synchronous variants are considered. The optimisation parameters are orbit RAAN and initial Greenwich meridian and the objective function is defined as the quantity of total energy

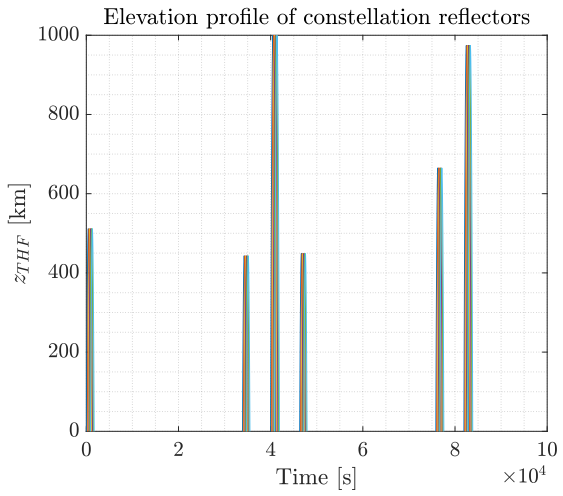

(a) All-day view

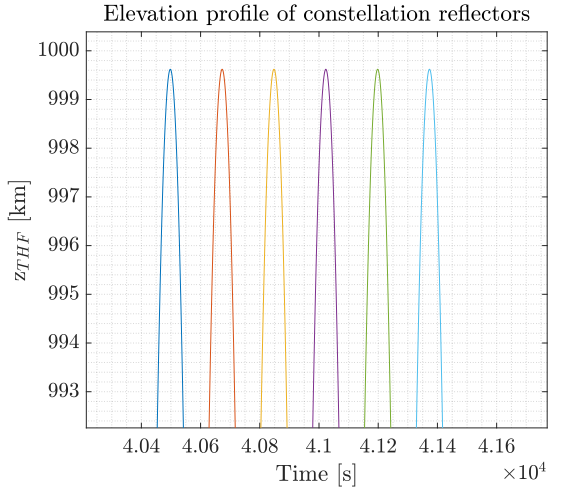

(b) Zoomed-in view at approximately 12th hour

Fig. 2. The elevation profile of a constellation reflectors in six orbit planes, distributed according to Eq. (23).

generated per day. The details of the optimisation process will be explained later. For both polar and Sun-synchronous orbits, two optimisation cases are investigated. The first is a single reflector in the aforementioned orbit, initially at mean anomaly $M = 0\,\text{deg}$. The second case is a two-reflector configuration, both in the same orbit with $180\,\text{deg}$ apart in mean anomaly, i.e., $M_{11} = 0\,\text{deg}$ and $M_{12} = 180\,\text{deg}$. The latter case aims at a dawn/dusk cluster of orbits when expanded with multiple orbit planes to create a constellation. Recall that the setting of the constellation problem in Eqs. (23) and (24) ensure that reflectors in subsequent orbits would follow the same pass geometry over the solar power farms as the reflectors in the first orbit. Before the details of the optimisation process is presented, first the selection of the solar power farms will be summarised.

4.1. Solar power farms

Solar power farms (SPF) in this paper are selected from some of the largest operational and under-development projects with nameplate capacity greater than 500 MW as of 2020, first summarised in Viale et al. (2023) [12] and updated to the current known capacity and land size values in this paper. In addition, this paper also considers a number of hypothetical solar power farms. The potential benefits

Table 2
Selected solar power farms in this paper [12]. The land size and capacity information are updated to the latest values available.

#	Solar power farm (SPF)	Capacity [MWh]	Land size [km^2]	Coord. (lat., lon) [deg, deg]
Existing solar power farm projects				
1	Bhadla	2700	160	27.5, 71.9
2	Pavagada	2050	53	14.7, 77.2
3	Benban	1650	37	24.7, 32.8
4	Tengger	1547	43	37.6, 105.04
5	Noor Abu Dhabi	1177	8	24.6, 55.4
6	Datong	1070	N/A	40.7, 113.1
7	Kurnool	1000	24	16.15, 78.4
8	Longyangxia	850	14	36.9, 100.5
9	Villanueva	828	24	26.3, −102.9
10	Solar Star I&II	747	13	35.8, −118.15
11	Topaz	550	19	34.4, −115.2
12	Sun Cable	6000	105	−17.29, 133.5
Hypothetical solar power farms				
13	SPF-13	–	78.5	35, 89.45
14	SPF-14	–	78.5	24.73, 6.42
15	SPF-15	–	78.5	24.73, −19.91
16	SPF-16	–	78.5	−5, -32
17	SPF-17	–	78.5	0,-128
18	SPF-18	–	78.5	0, -154
19	SPF-19	–	78.5	−24, 150
20	SPF-20	–	78.5	−24, 118

of additional solar power farms that are strategically placed near the groundtrack of a selected reflector orbit and high-insolation regions were previously discussed in Viale et al. (2023) in enhancing the terrestrial solar energy generation [12]. In this paper, this will be considered alongside existing solar power farm projects to assess that enhancement. The SPF considered in this paper are presented alongside a yearly mean insolation map (covering 1990–2004) in Fig. 3.

Fig. 3 shows how the existing SPF projects are placed in favourably insolated geographical locations. For hypothetical farms, a similar approach is taken, but longitudes of hypothetical SPF are also chosen by considering the longitudinal shift of the ground track on the surface of the Earth after each orbit. Considering eastward Earth rotation at a rate of ω_E and westward rotation due to the J_2 effect, $\dot{\Omega}_{J_2}$, the orbit ground track would shift approximately $(\omega_E - \dot{\Omega}_{J_2})T_{J_2}$. As will be outlined in the next section, the orbit altitude will be $1000\,\text{km}$, which means that the westward groundtrack shift for a Sun-synchronous orbit and polar orbit at this altitude would be $26.7\,\text{deg}$ and $26.3\,\text{deg}$, respectively. Therefore, the longitudinal separation between two consecutive hypothetical SPFs is considered to be $26.7\,\text{deg}$ as SSOs are more relevant for orbiting solar reflector applications and considering the small difference between the values. Latitudinal placement is more related to nearby existing SPF, insolation properties, proximity to land and generally attempting to avoid an orbit groundtrack passing over multiple farms at the same time (or in quick succession) to ensure distinctive passes and the maximal use of all SPFs. The locations of the SPF are listed in Table 2.

The existing solar farm projects are dominantly in the northern hemisphere, with a number of large SPF in India, China, and USA together with single farms in UAE and Egypt. Among the large projects considered, the Sun Cable SPF project is the only one in the southern hemisphere, which is currently under development and may potentially be one of the largest SPF in the world with a nameplate capacity of 6 GW. Among the hypothetical SPF, two each are placed in North Africa, Australia and the equatorial regions of the Pacific and one each in western China and the eastern tip of Brasil. The most geographically remote SPF are in the Pacific (SPF-17 and SPF-18) and offshore, but they are also in very high insolation regions, which may be considered to provide electricity to Pacific island countries or Hawaii if a higher latitude is considered. Two hypothetical SPF in Australia (SPF-19 and SPF-20) are at the two edges of the country, while the existing project

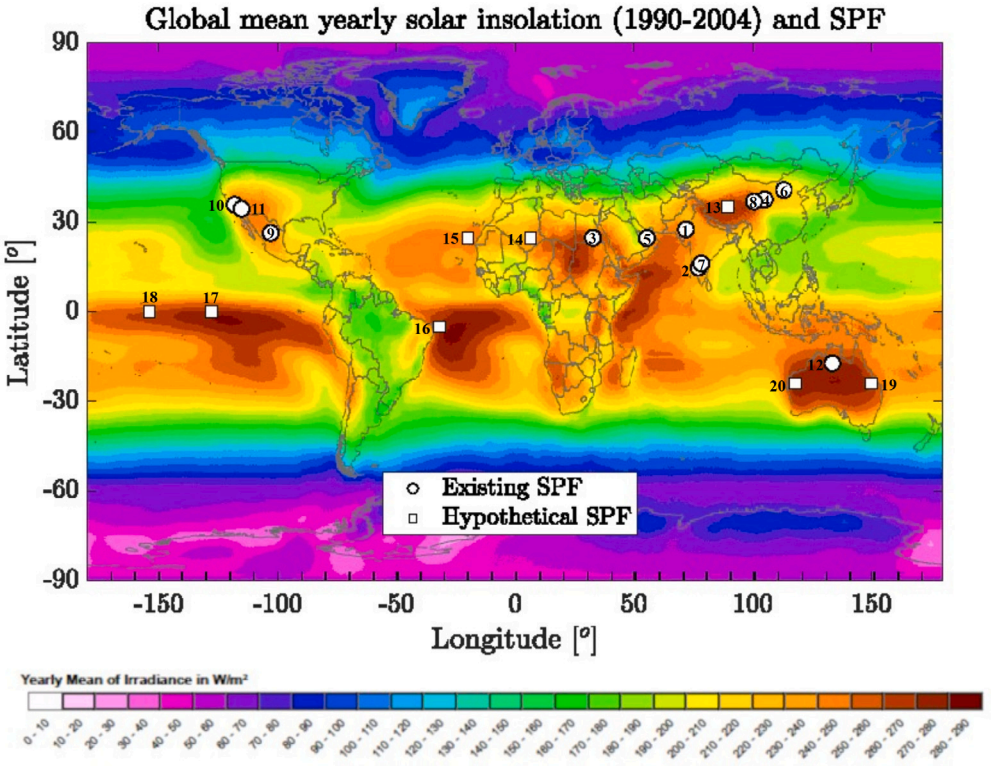

Fig. 3. Existing and hypothetical solar power farms on global yearly mean insolation map 1990–2004. The insolation map is freely available at https://www.soda-pro.com/maps/maps-for-free (Accessed March 3, 2022).

Sun Cable is at the north, potentially providing electricity all around the country. One of two farms in North Africa (SPF-15) and the one in Brasil (SPF-16) are offshore due to longitudinal separation, although both are still very close to land. The one selected in western China (SPF-13) is likely in a high-altitude region, but solar energy experiences less atmospheric transmission losses in high altitudes [21], which may be preferable from that perspective. The selection of hypothetical SPF also increases the number of opportunities all around the globe, particularly in the southern hemisphere. Ultimately the optimisation of groundtracks will demonstrate their effectiveness, whose process is outlined in the next subsection.

4.2. Optimisation process

The optimisation process is as follows: First, for given orbit parameters, the orbit pass geometry is calculated for 24 h in terms of its elevation angle for each of the solar power farms presented in Table 2. This check is performed by using analytical elevation formulations presented in Eq. (3) and in Ref. [20]. If the maximum elevation angle is greater than 60 deg at any point during the day, these instances are recorded and the pass duration is calculated for that pass. It is expected that such a pass could occur twice per day per reflector at the maximum, at dawn and dusk each. If no pass over the selected solar power farm reach a maximum elevation angle greater than 60 deg, then that solar power farm is considered not serviced by the reflector on the given orbit.

For the passes that satisfy the 60 deg requirement, the quantity of energy delivered is calculated. This follows the procedures discussed in Çelik & McInnes (2022, 2023) with the equations presented in Section 2 and includes the Earth's rotation and oblateness, geometric and atmospheric losses in the energy delivery process [16,20].

This procedure is performed for all reflectors (if there is more than one) and for all solar power farms. Finally, the quantity of total energy delivered per day is calculated. The procedure of calculating the optimised orbit is presented in Fig. 4.

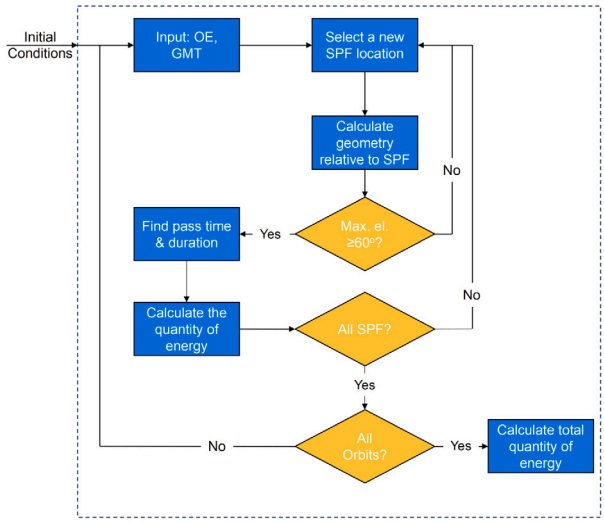

Fig. 4. Diagram of the optimisation process. OE and GMT denote orbital elements and Greenwich mean time respectively.

One limitation of this approach is the existence of solar power farms that are located very close to each other. The examples include Bhadla (SPF-1), Pavagada (SPF-2) and Kurnool (SPF-7) farms in India or Villanueva (SPF-9), Solar Star I/II (SPF-10) and Topaz (SPF-11) farms in Mexico and the United States. It was observed that often the same orbit groundtrack passes over both of those targets satisfying the 60 deg requirement, hence the quantity of energy delivery is overcalculated within the optimisation function. This is not necessarily a problem, however, as one of those overlapping passes will indeed provide the highest quantity of energy delivered, which is considered while the others are removed as infeasible in the post-processing.

Table 3
Parameters of the optimisation problem.

Orbital parameters	
Altitude [km]	1000
Eccentricity [–]	0
Inclination [deg]	90 (Polar), 99.5 (SSO)
Reflector parameters	
Diameter [km]	1
Reflectivity [–]	1
Solar power farms	
Diameter [km]	10
Location	Table 2
Optimisation parameters	
Objective function	$-E_{\text{tot}}$
Variables [deg]	$\Omega \in [90-\beta,\ 90+\beta-\eta_\Omega]$ $\theta_{G,0} \in [-45,\ 30]$

As noted earlier, the objective is to maximise the total quantity of energy delivered per day, and the two optimisation parameters are the right ascension of the ascending node of the orbit, Ω and the initial Greenwich meridian, $\theta_{G,0}$. The latter parameter appears relatively arbitrary as it only determines when the orbit starts during a day, but it will be shown that there are multiple optima available in the problem based on different Ω-$\theta_{G,0}$ combinations. The range of Ω is selected based on the eclipse considerations and a range extending by β on either side of the terminator line defined at $\pi/2$ from the x-axis in the ECI frame. The upper limit of Ω is also reduced by an angle of η_Ω, such that if the optimised Ω is found in this upper limit, it would still be possible to place the rest of the constellation reflectors without any eclipses. To that end, it is necessary to determine the number of orbit planes, N_o, before the optimisation to calculate η_Ω with Eq. (20) to set the upper limit of Ω. In this paper, $N_o = 10$ is selected. As for $\theta_{G,0}$, the range is selected between -45 deg and 30 deg measured from the x-axis in the ECI frame or approximately 9:00 am-2:00 pm GMT. The upper limit is kept at 30 deg to avoid Ω being pushed to the upper limit during the optimisation process. The other parameters including the orbital elements used in the optimisation are presented in Table 3.

The single-objective optimisation is performed using a genetic algorithm [25] and implemented in MATLAB through its `ga()` function.[1] The genetic algorithm relies on evolutionary principles and aims to reach the best result (or global optimum) via stochastically generated populations through their crossovers and mutations. It is widely used in constellation optimisation problems where the best distribution of satellites minimising an objective function is not apparent or trivial. In the problem here, even though the optimisation does not contain many reflectors, the pass geometry over the listed solar power farms and the associated quantity of energy deliverable to those cannot be found trivially. In the absence of this information, the genetic algorithm becomes a suitable choice. As for different options available for `ga()` in MATLAB, initial parameter space is created based on a uniform distribution with scattered crossover and stochastic uniform selection of parents at each step. For the mutations, an adaptive feasible mutation option is selected, which generates random search directions and is adaptive to the success of each generation. The function and constraint tolerances are 10^{-6} and 10^{-3}, respectively. The rest of the options are used as default in `ga()` in MATLAB. By using the procedures and tools explained in this section, groundtrack optimisation is performed, and whose results are presented in the next section.

[1] Available at https://uk.mathworks.com/help/gads/ga.html, Accessed August 29, 2023.

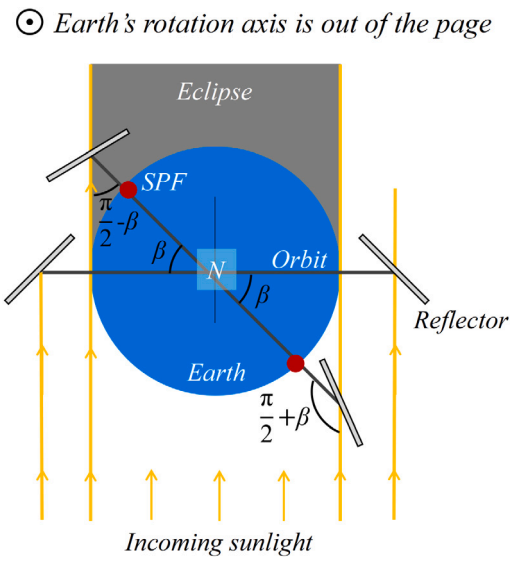

Fig. 5. Variation in energy delivery in polar orbits as a result of the change in right ascension of the ascending node (Ω) of the orbit. For a non-rotating Earth, the angle of incidence ψ would be near constant and related to Ω by a cosine relationship. This means that the quantity of the solar energy delivered to the night side of the Earth would be greater than that of day side.

5. Optimised orbits and their properties

The orbit optimisation is performed for polar and Sun-synchronous orbits, which are also near polar at 99.5 deg inclination, as presented in Table 3. Considering the stochastic nature of the set of initial conditions and generated populations in the genetic algorithm, each groundtrack optimisation is performed 10 times and the results are post-processed to obtain the total quantity of energy delivered in each case. Then, the orbit is selected not only based on its highest quantity of energy delivered but also its Ω value. These aspects will be discussed in the next subsections together with the results.

5.1. Polar orbits

5.1.1. Single reflector

The optimisation results of the polar orbits are presented in Table 4.

Table 4
Polar orbit results.

#	$\theta_{G,0}$ [deg]	Ω [deg]	E_{tot} [MWh]	$E_{tot,pp}$ [MWh]
1	14.45	85.98	453.1	334.2
2	−6.81	64.73	454.3	334.7
3	22.88	94.42	452.6	333.7
4	17.54	89.08	452.9	333.9
5	11.26	82.80	453.3	334.3
6	14.02	85.56	453.1	334
7	28.36	99.91	452.3	333.3
8	2.34	73.88	453.8	334.7
9[a]	15.90	87.45	453.0	334
10	3.22	74.76	453.7	334.6

[a] Solution is selected for further investigation.

The results show the existence of multiple local optima depending on different $\theta_{G,0} - \Omega$ pairs, with the total quantity of energy (unprocessed) ranging between 452.3 and 454.3 MWh. As the Earth's rotation is included in the problem, it may be reasonable to find such close results with adjustments in $\theta_{G,0}$ and Ω. The highest E_{tot} values in this range is at $\Omega = 64.73$ deg, close to the lower bound of the optimisation range, 59.82 deg. The push in the solution towards this edge may be

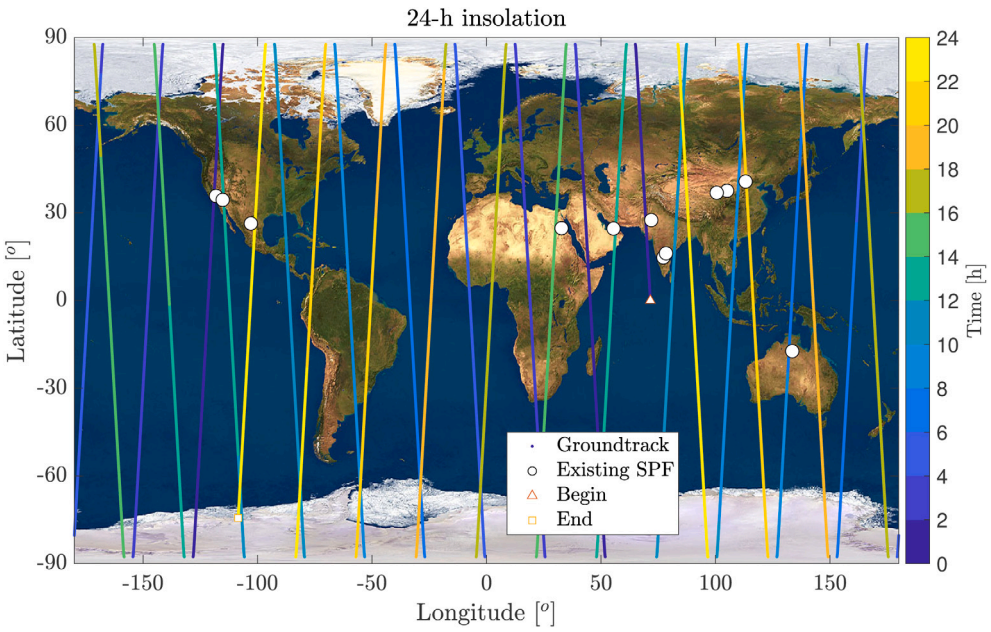

Fig. 6. 24-h groundtrack of the selected optimal polar orbit.

explained by the geometry of the energy delivery in polar orbits. As a simplified case, if a non-rotating Earth is assumed, a reflector satellite passing over a solar power farm would have a fixed angle of incidence with respect to the Sun, as shown in Fig. 5.

It can be seen in Fig. 5 that the angle with respect to the Sun increases as the satellite on the day side and decreases on the night side. The implication of this is that according to Eq. (1) the quantity of power delivered at any instant would be increased on the night side and decreased on the day side. For the solution with the highest quantity of energy delivered, Ω is closest to the lower bound of the optimisation problem, suggesting that more passes are encountered on the night side when the incidence angle is smaller. Some of the other solutions in Table 4 with higher E_{tot} also have lower Ω values, e.g. Solution #8 and #10. Conversely, if this reasoning holds, then Ω values closer to upper bound should result in lower E_{tot} values, which what is seen, for example, in Solution #3 or #7. However, it should be noted that this best solution is only slightly higher in the final E_{tot} compared to the rest of the solutions. This increase ultimately becomes more marginal when the results are post-processed to remove overlapping passes of close-by solar power farms. The post-processed quantity of total energy delivered per day, $E_{tot,pp}$, varies only by 1.4 MWh, between 333.3 MWh and 334.7 MWh. It was found that the sequence of passes is the same in all solutions. However, instead of simply selecting the highest $E_{tot,pp}$, an orbit closer to the terminator line (i.e., $\Omega = 90\,\text{deg}$) is also considered, and Solution #9 is selected for further in-depth investigation. The ground track of this orbit is presented in Fig. 6.

This orbit groundtrack shows multiple near-overhead passes that deliver the highest quantity of energy. These appear to be populated around the solar power farms in North America, but other passes also exist in China, India and Australia. Fig. 7 depicts the daily distribution of these passes.

In Fig. 7, the horizontal axis shows the elapsed time since the beginning of the propagation whereas the vertical axis shows the elevation from the topocentric horizon frame of the solar power farm in degrees. The spike-like appearance of the data is due to the short duration of passes (~17 min) compared to the 24-h simulation time. All solar power farms listed in Table 2 are visible to the reflector during a day, but due to the close proximity of some of the solar power farms, some passes overlap. These are apparent particularly between SPF-10 and SPF-11. The former is more favourable in the first instance whereas the latter is

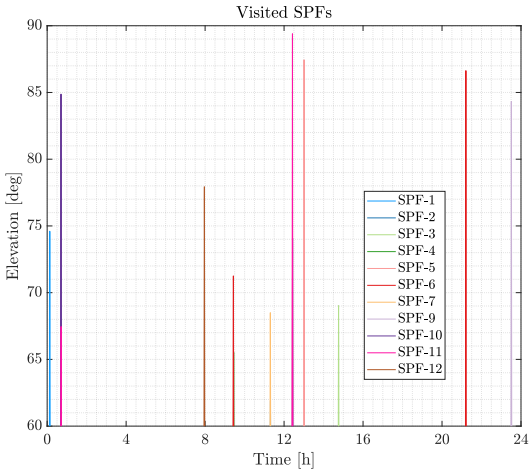

Fig. 7. Elevation profile of passes in the selected optimal polar orbit. Single reflector case.

more favourable approximately half a day later. Indeed the second pass is almost overhead with maximum elevation reaching nearly 90 deg. The other overlapping passes are less apparent but between SPF-6 and SPF-4, and SPF-7 and SPF-2 where the geometry is more favourable for SPF-6 and SPF-7 in these cases. When such overlapping passes occur, the one with the higher quantity of energy delivered in post-processing is selected as more than one solar power farm cannot be serviced. Detailed schedule of the passes are provided in Table 5.

Ultimately a total of 10 distinct passes can be achieved with SPF-6 visited twice. Five of those are with a maximum elevation greater than 80 deg, which is one more than previously achieved with Sun-synchronous orbits in Viale et al. (2022) [12]. The total quantity of energy delivered to these farms is 334 MWh, which is also approximately 18% higher than previous results [12], improving the viability of orbiting solar reflectors.

5.1.2. Dawn/dusk reflectors

The second investigation with polar orbits is a case of two reflectors in one orbit, one placed at $M_{11} = 0\,\text{deg}$ and the other placed at

Table 5
Polar orbit pass sequence results.

SPF #	T_{pass} [min]	ϵ_{max} [deg]	E [MWh]
1	16.77	74.6	32.7
10	17.56	84.9	34.8
12	17.54	77.9	33.9
6	17.45	71.3	32.0
7	17.50	68.5	30.4
11	17.56	89.3	34.9
5	17.56	87.4	34.9
3	17.46	69.0	31.0
6	17.57	86.6	34.8
9	17.56	84.3	34.6
Total			334.0

Table 6
Polar orbit dawn/dusk results.

#	$\theta_{G,0}$ [deg]	Ω [deg]	E_{tot} [MWh]	E_{11} [MWh]	E_{12} [MWh]	$E_{tot,pp}$ [MWh]
1	−28.87	94.77	744	295	269.2	564.2
2	−28.43	106.88	742.8	261.2	301.4	562.6
3	−9.44	94.65	742.9	261.3	301.8	563.1
4	7.33	63.52	743	261.7	301.6	563.3
5	−38.10	85.79	745.6	268.1	265.3	533.4
6	−25.16	81.80	742.8	261.2	301.6	562.8
7	28.17	114.61	745	297.1	267.1	564.2
8	−17.89	61.01	746	268.6	265.5	534.1
9[a]	5.78	95.37	744.5	296.3	268.2	564.5
10	−9.95	67.43	746.1	268.8	265.5	534.3

[a] The solution is selected for further investigation.

$M_{12} = 180$ deg. This is essentially a basic constellation on a single orbit, selected to service both dawn and dusk times. Again the optimisation is performed 10 times to consider the stochastic nature of the genetic algorithm. The results are presented in Table 6.

Table 6 also includes the post-processed results of individual reflectors, E_{11} and E_{12}. The total quantity of energy delivery has increased due to two reflectors, but the quantity of energy delivered *per* reflector is effectively decreased. On average, E_{tot} per reflector is approximately 372 MWh before post-processing, which decreases to approximately 282 MWh after post-processing. This difference may be explained by the proportion of solar power farms in the eastern and western hemispheres of the Earth. Of the existing largest solar power farms in Table 3, only three are in the western hemisphere. Therefore, it is possible that one reflector has always fewer opportunities to deliver energy, whereas the passes of the other may overlap with multiple farms, of which only one can be chosen.

When individual reflectors are considered, it appears that there are several different solution combinations that lead to approximately the same result. For example, for Solutions #1 and #9, the first reflector delivers more energy ($E_{11} > E_{12}$), for Solutions #2, #3, #4 and #6 the second reflector delivers more ($E_{12} > E_{11}$) and there are two other solutions where the energy delivery is similar for both reflectors (Solutions #5 and #10), which in total deliver the least quantity of energy. These different solution structures also result in different sequences of solar power farm visits. Within similar solutions, the orbit placement also differs with different $\theta_{G,0} - \Omega$ pairs.

Again, given the similarity between most of the solutions in terms of $E_{tot,pp}$, Solution #9 is selected for further investigation due to its proximity to the terminator line. Only the elevation angle properties of the individual reflectors will be shown in Fig. 8 for conciseness.

The arguments made about the solutions obtained and the proportion of solar farms in the eastern and western hemispheres of the Earth may be more apparent in Fig. 8. First reflector ($M_{11} = 0$ deg) has only three passes that exceed a maximum elevation of 80 deg and one of them only slightly exceeds that point. No elevation is greater than 85 deg. There are also several overlapping passes towards the end of the day, which decreases the overall total quantity. On the other hand, the second reflector has only four passes that exceed the 80 deg mark (three greater than 85 deg), but does not visit any solar power farm until the 7th hour of its operation. Ultimately, however, the first reflector visits more targets and delivers more energy between the two. The total number of distinct visits is equal to 17, of which 9 is achieved by the first reflector and 8 for the second, individually delivering 296.3 MWh and 268.2 MWh, respectively. This is less than what a single reflector can achieve (10 per day) as discussed in the previous subsection. The single reflectors then demonstrate superior performance compared to the two-reflector dawn/dusk configuration in one orbit for the polar orbit case. This discussion can be extended to Sun-synchronous orbits, which are more relevant for orbiting solar reflector applications.

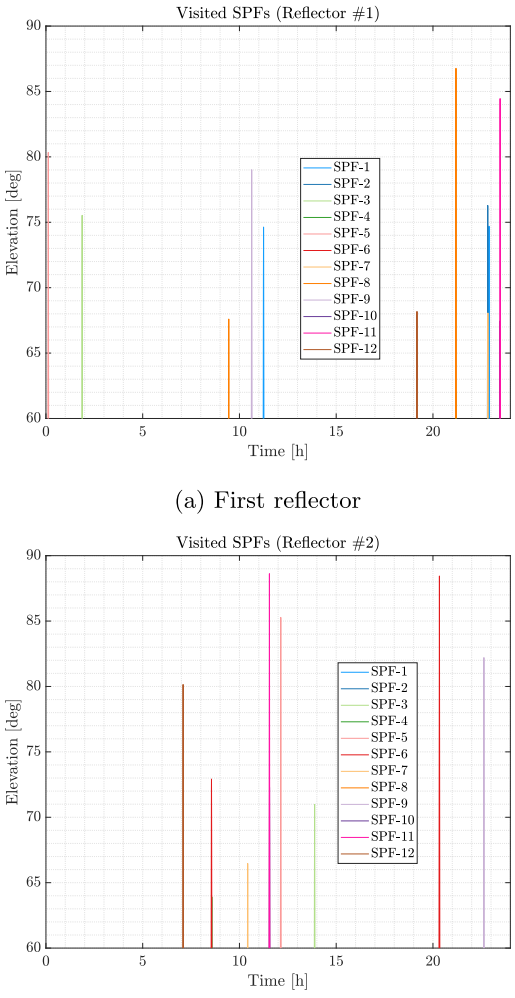

(a) First reflector

(b) Second reflector

Fig. 8. Elevation profile of passes in the selected optimal polar orbit. Dawn/dusk case.

5.2. Sun-synchronous orbit

5.2.1. Single reflector

Sun-synchronous orbits (SSO) would provide a more favourable choice for solar reflector applications [12] as the orbit plane tracks the Sun's direction through the perturbation due to the Earth's oblateness. Considering this, the optimisation is performed with the parameters in Table 3 for 10 times and the results in Table 7 are obtained.

The SSO results demonstrated a more uniform solution that does not differ much in terms of E_{tot} (the maximum difference is 0.3 MWh), but

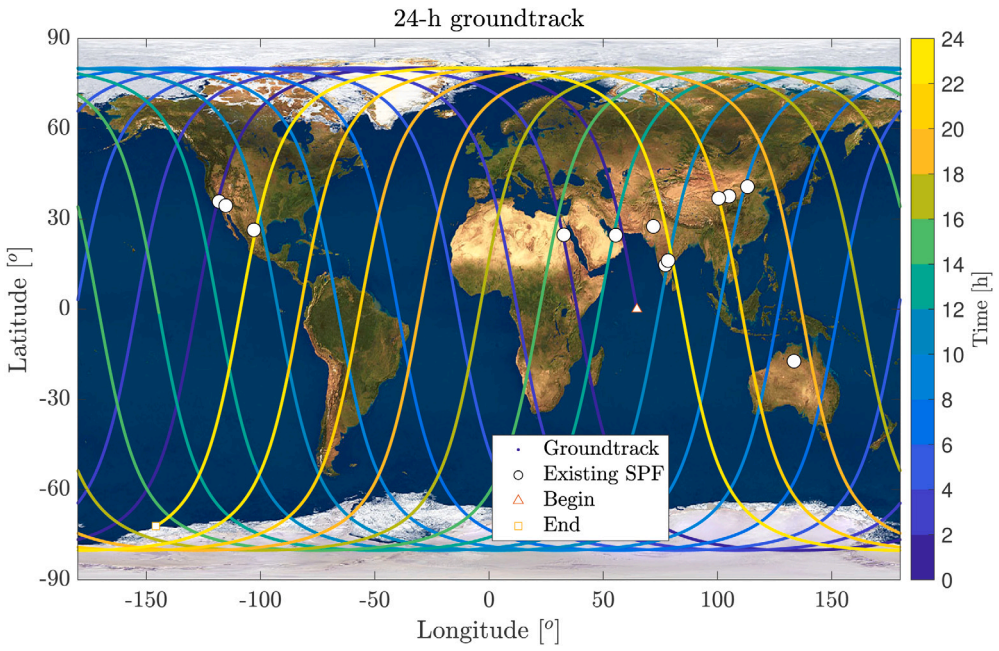

Fig. 9. 24-h groundtrack of the selected optimal Sun-synchronous orbit.

Table 7
SSO optimisation results.

#	$\theta_{G,0}$ [deg]	Ω [deg]	E_{tot} [MWh]	$E_{tot,pp}$ [MWh]
1	17.31	82.04	537.1	363.4
2[a]	27.59	92.32	537.0	363.5
3	26.02	90.75	537.0	363.3
4	16.01	80.74	537.1	363.4
5	−1.59	63.14	537.3	362.6
6	9.85	74.58	537.2	363.3
7	18.53	83.26	537.1	363.5
8	8.96	73.69	537.2	363.4
9	0.19	64.92	537.3	362.7
10	−2.09	62.63	537.3	363.4

[a] The solution is used for further investigation.

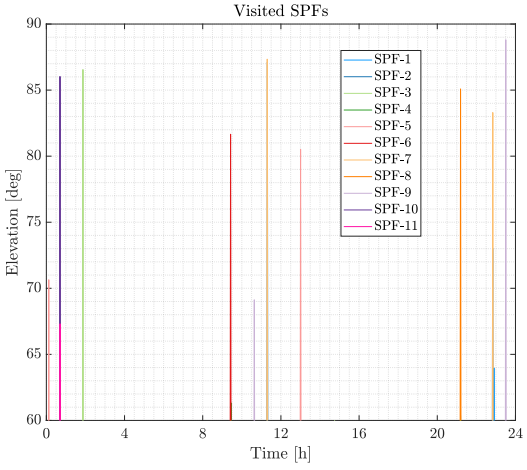

Fig. 10. Elevation profile of passes in the selected optimal Sun-synchronous orbit. Single reflector case.

again multiple local optima are available. Due to the inclined orbits and the pertubation due to Earth's oblateness, the incidence angle is not constant and the arguments about the incidence angle (see Fig. 5) discussed for polar orbits appear less prevalent to explain the similarity in E_{tot} throughout the given range of lower and upper bounds [12]. The post-processed results show slightly more variation (0.9 MWh) but the variation is still less than the polar orbit case. Therefore, solution #2 is selected for further investigation. The ground track of this orbit is presented in Fig. 9.

An immediate qualitative comparison can be made between SSO in Fig. 9 and polar orbit groundtracks in Fig. 6, where the SSO groundtrack visits more solar power farms and of which more appear to be close to overhead. Indeed, it appears that nearly all solar power farms have close-by groundtracks, except Sun Cable (SPF-12), which may still be visible albeit with a maximum elevation lower than that of required in this paper, i.e., $\epsilon_{max} \geq 60\,\text{deg}$. The elevation angle for all passes can be seen in Fig. 10.

Indeed Fig. 10 shows 9 passes with $\epsilon_{max} > 80\,\text{deg}$ (5 over 85 deg, also reported in Table 8), which is almost double that of the polar orbits. However, there is almost an exact overlap between SPF-7 and SPF-2 around the 12th hour mark, where the passes demonstrate almost the same elevation properties, although, in the end, SPF-7 exhibits better opportunity in terms of the quantity of energy delivered. Therefore, only 8 passes are available with $\epsilon_{max} > 80\,\text{deg}$. In total, 11 distinct passes satisfy the $\epsilon_{max} \geq 60\,\text{deg}$ requirement and a total of 363.5 MWh of energy is delivered. This is more than the polar orbit case in the previous subsection, although the difference is approximately one pass more on average with the additional pass over SPF-1 being at low elevation. However, as noted earlier SSO provides more favourable properties over yearly operations.

When compared with the reference architecture study presented by Viale et al. (2023) [12], the optimal SSO in this paper presents a significant improvement in daily operations. Despite using a smaller reflector (1 km diameter in this paper vs. 1.016 km effective diameter in Ref. [12]) and a higher altitude (which reduces the solar power density), the quantity of energy delivered per day is increased by approximately 28% (363.5 MWh in this paper vs. 283.84 MWh in Ref. [12]). The difference between this paper and Viale et al. (2023) [12] is that the orbit selection in the latter was motivated by anchoring the groundtrack to a particular solar power farm (SPF-12 in this paper), whereas in this paper the selection is motivated to maximise the daily energy delivery globally.

Table 8
SSO pass sequence results.

SPF #	T_{pass} [min]	ϵ_{max} [deg]	E [MWh]
5	16.11	70.6	31.4
10	17.35	86.0	34.3
3	17.36	86.5	34.3
6	17.33	81.7	33.9
9	17.25	69.1	30.7
7	17.34	87.3	34.4
5	17.32	80.5	33.8
8	17.37	85.1	34.2
7	17.33	83.3	34.2
1	17.12	64.0	27.9
9	17.35	88.8	34.4
Total			363.5

The SSO analysis can also be extended to the dawn/dusk two-reflector case, which is discussed next.

5.2.2. Dawn/dusk reflectors

The optimisation results of the two-reflector case in SSO are presented in Table 9.

Table 9
SSO dawn/dusk results.

#	$\theta_{G,0}$ [deg]	Ω [deg]	E_{tot} [MWh]	E_{11} [MWh]	E_{12} [MWh]	$E_{tot,pp}$ [MWh]
1	−5.07	77.4	730.2	228.1	285.2	513.3
2	−15.14	70.22	757.3	225	325.4	550.4
3	18.0	64.52	758.5	226.6	325	551.6
4	−27.61	95.14	756.8	224.4	325.3	549.7
5	−2.13	76.73	757.7	224.4	325.3	549.7
6[a]	−10.13	95.44	757.4	224.4	325.4	549.8
7	−31.85	101.35	756.7	224.3	325.7	550
8	24.75	77.20	758.7	224.4	325.2	549.6
9	−35.47	69.87	756.6	224.3	325.3	549.6
10	16.46	77.06	758.4	224.4	325.1	549.5

[a] Solution is selected for further investigation.

The quantity of total energy delivered by the two reflectors in SSO is higher than that of the same case in polar orbits (except Solution #1 in Table 9) before post-processing. But this may be a misleading result as the post-processed results indeed show a decrease below the values achieved by polar orbits, except polar orbit Solutions #5 and #8. The overall decrease in the two-reflector cases in both SSO and polar orbits may be explained by the disproportionate distribution of solar power farms in the eastern and western hemispheres of the Earth, but the decrease in SSO as compared to polar orbits is not directly evident. A possible explanation could come from the single reflector results in Fig. 10. Indeed the pass geometries, in general, are much better with ϵ_{max} exceeding 80 deg for several solar power farms. But there are also more overlapping passes with similar elevation profiles, such as between SPF-10 and SPF-11 or SPF-7 and SPF-2, in which the latter overlaps twice in a day, as shown in Fig. 10. These are not distinguished during the optimisation process, therefore the value of the objective function is maximised by these overlaps, even though the actual result will be lower. But if the overlapping passes are of the same high quality, then the decrease will also be greater when these overlaps are removed. This may be a potential explanation for the initially higher E_{tot} but finally lower $E_{tot,pp}$ values in the SSO case as compared to polar orbits. Nevertheless, it should also be noted that the difference between the SSO and polar orbit cases is only approximately 15 MWh at the maximum, which is less than one overhead pass equivalent quantity of energy, i.e., approximately 35 MWh from earlier analyses [16,20].

For all the solutions presented in Table 9, the second reflector always delivers more energy (i.e. $E_{12} > E_{11}$) and all but one solution (solution #1) is different in terms of the visit sequence of solar power

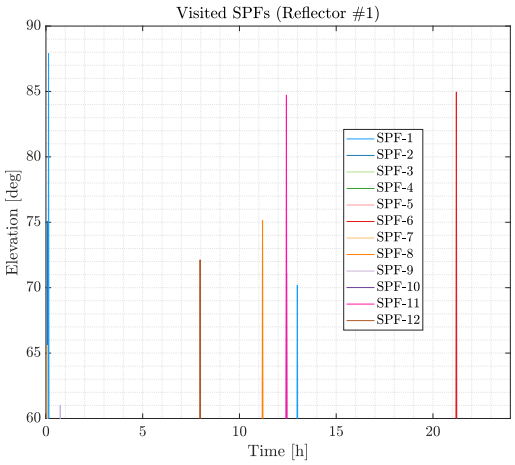

(a) First reflector

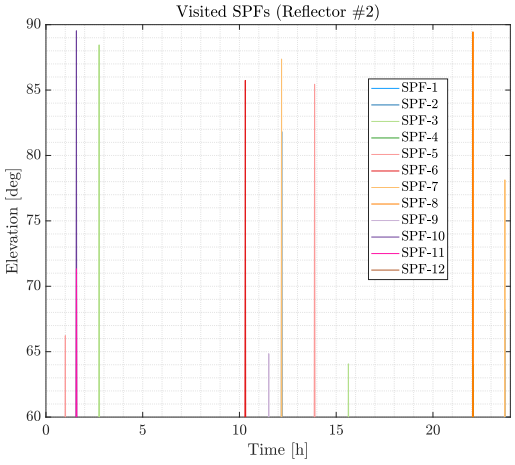

(b) Second reflector

Fig. 11. Elevation profile of passes in the selected optimal Sun-synchronous orbit. Dawn/dusk case.

farms. Therefore among similar solutions, Solution #6 is selected for further investigation and the elevation profiles of both reflectors are presented in Fig. 11.

Reflector #1 has only three passes that exceed 80 deg elevation, but there are a number of passes that overlap, which supports the argument made above. The very first pass has SPF-1, SPF-7 and SPF-2 overlapping, where SPF-1 provides the highest elevation. SPF-2 (ϵ_{max} = 75 deg) and SPF-7 (ϵ_{max} = 66 deg) need to be removed in this case but each delivers 31.5 MWh and 28 MWh, respectively. Similarly, the SPF-11 pass overlaps with the SPF-10 pass, where the latter's significant contribution (31.3 MWh) is also removed. The same occurs for the second reflector as well, where overlapping SPF-7 and SPF-2 passes both exhibit $\epsilon_{max} > 80$ deg and removing SPF-2 results in a significant loss (34 MWh) in final deliverable energy.

It appears that the proximity of some of the solar power farms has considerable effect on the total quantity of deliverable energy in both single and dawn/dusk reflector cases. Some of this may be overcome by strategically located solar power farms and the orbits servicing them, which will be analysed next.

5.3. Orbits optimised with hypothetical solar power farms

The same orbit optimisation is performed with the inclusion of hypothetical solar power farms as additional targets. Recall that the

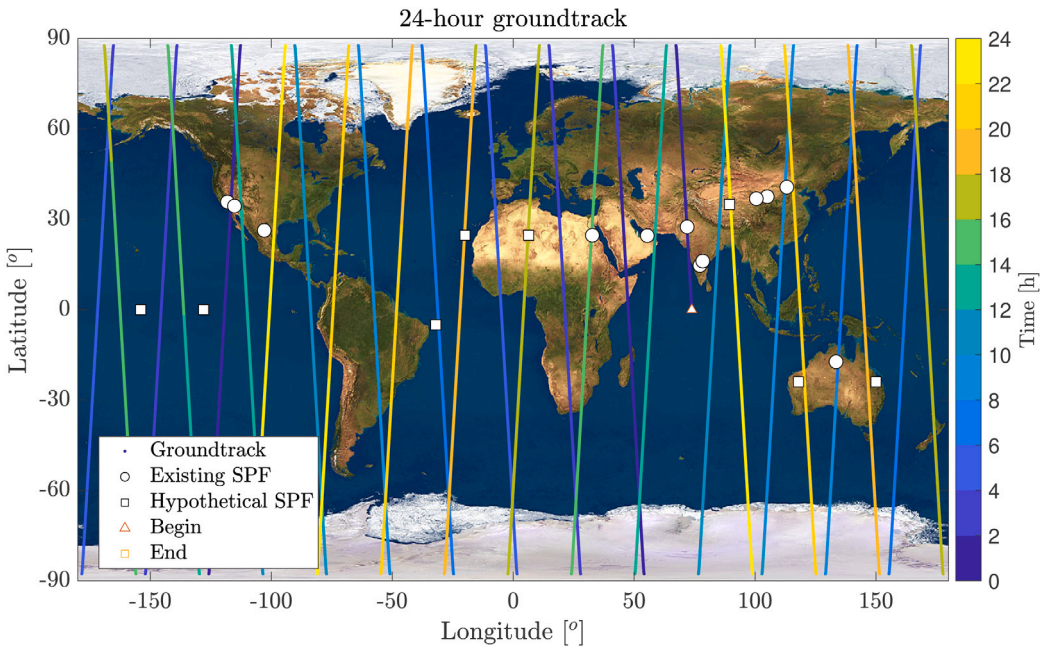

Fig. 12. 24-h groundtrack of the selected optimal polar orbit with hypothetical farms.

locations of solar power farms are primarily selected in highly insolated regions (see Fig. 3) with the longitudinal differences between them equal to the orbit groundtrack shift for a 1000-km altitude SSO. These criteria are informed from both the selected orbit and the day-time solar energy potential of these regions, allowing an overall increase in both day and nighttime utility of solar energy.

Given the inferior performance of dawn/dusk reflector systems in general, the optimisation was only performed for single reflectors in polar and Sun-synchronous orbits. Again, ten different optimisations were performed for both cases, but it was observed that the final results are similar and the pass sequences are the same for all solutions, therefore a detailed investigation of the solution structure will not be presented. Orbit groundtracks and a breakdown of the passes will be discussed instead. The selected solutions are presented in Table 10. Among them, the first groundtrack results are presented for polar orbits in Fig. 12.

As aimed at and expected, the number of passes during the day increases with a significant number of near-overhead passes. The hypothetical solar power farms in North Africa, Australia, Brasil and China have all been targeted. The SPFs in the Pacific have not been targeted in the optimisation with polar orbits for near-overhead passes. Fig. 13 shows the details of the elevation profiles of all passes.

Among all 20 existing and hypothetical SPFs, 16 of them are available for energy delivery, though some of the passes either overlap or are too close to each other to service them all. Ten of them achieve maximum elevation greater than 80 deg. Again SPF-10 and SPF-11 have overlapping passes, where SPF-10 is selected as it provides better geometry. Other notable passes include SPF-1 that reaches $\epsilon_{max} > 89$ deg and SPF-13 reaches $\epsilon_{max} > 85$ deg. Table 11 shows the breakdown of the passes and the quantity of energy delivered in each pass.

A total of 16 passes are available in a day that reaches higher than 60 deg elevation in a day. At the chosen orbit altitude (1000 km), a reflector would complete 13.7 orbits in a day, which means that some passes are in the same orbit. From Figs. 12 and 13 and Table 11, it appears that for example SPF-13 and SPF-11, and SPF-1 and SPF-10 share the same orbit on the opposite sides of the Earth. An earlier study showed that these may still be achievable as on average 6 min is sufficient for the reflector to reorient itself for the next pass [12]. The quantity of energy delivered is greater than 34 MWh for the majority of the passes with the minimum being 28 MWh (SPF-19) and the total quantity of energy per day is 534.4 MWh. Compared to the quantity in the single reflector case with existing SPF in the previous subsection (E_{tot} = 334 MWh), this is a 60% increase in the quantity of energy delivered for 67% increase in the number of SPF (from 12 to 20). The nearly linear increase in the quantity of energy delivered benefits from the strategic selection of locations of solar power farms. In comparison to the reference architecture study by Viale et al. [12], this represents an 88% increase in the quantity of energy that can be potentially delivered per day.

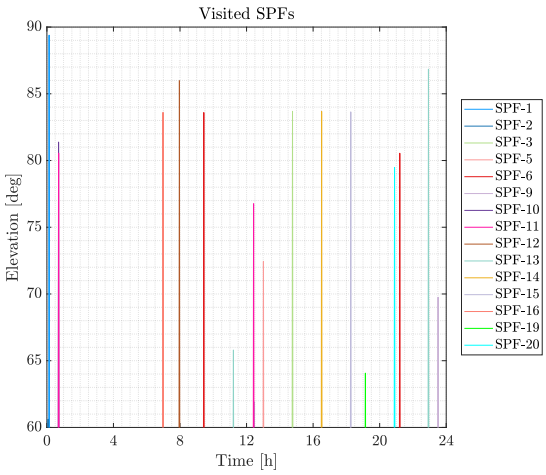

Fig. 13. Elevation profile of passes in the selected optimal polar orbit with hypothetical SPF included.

Table 10
The selected optimal solutions for further investigation.

Orbit	$\theta_{G,0}$ [deg]	Ω [deg]	E_{tot} [MWh]	$E_{tot,pp}$ [MWh]
Polar	14.16	88.01	621.3	534.5
SSO	24.03	89.51	859.9	588.4

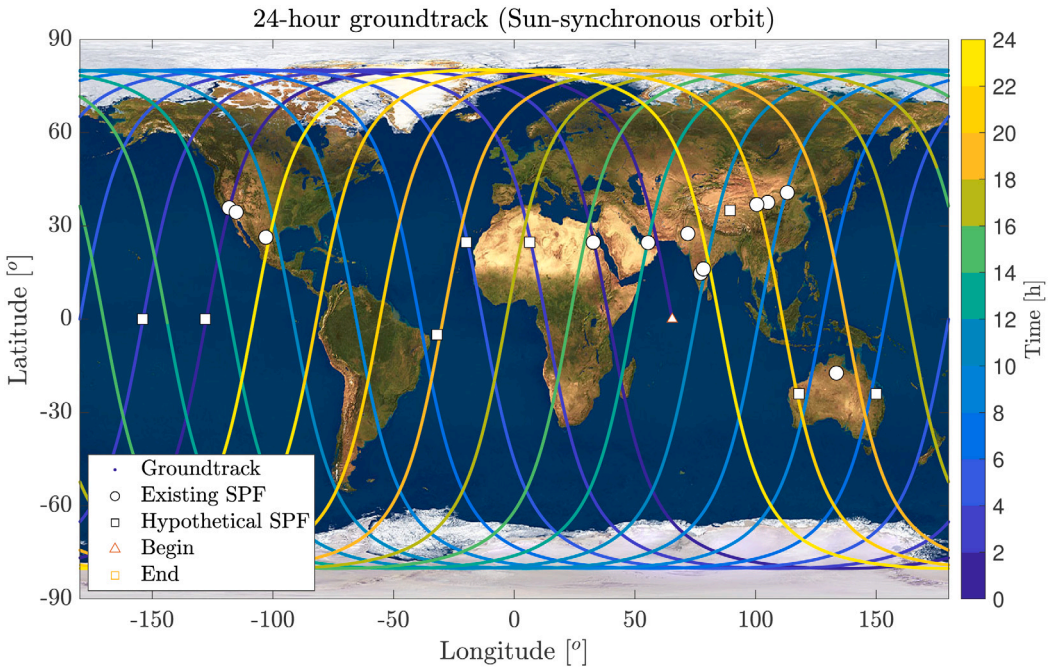

Fig. 14. 24-h groundtrack of the selected optimal SSO with hypothetical farms.

The next investigation will be for Sun-synchronous orbits with hypothetical solar power farms. The orbit groundtrack is shown in Fig. 14.

Qualitatively, Fig. 14 shows a much better use of solar power farms by the SSO. All listed SPF appear to have a part of groundtrack passing nearby, once or twice a day. Some passes again overlap where more favourable ones are chosen. The elevation profiles for all passes are shown in Fig. 15.

Fig. 15 shows that all passes except Sun Cable SPF (SPF-12) are available. Considering multiple passes over certain SPF, the total number of passes in a day is equal to 24, which is greater than the number of existing and hypothetical SPF listed (20). However, ultimately 18 distinct passes are feasible when considering the overlaps and very closely spaced sequences. Again, 18 passes mean that some passes are in the same orbit at the opposite sites of the Earth. 11 of those passes have $\epsilon_{max} > 85$ deg, meaning the passes are near-overhead with a near-maximum quantity of energy delivery. Among the existing solar power farms, SPF-3, SPF-5, SPF-7 and SPF-9 and among the hypothetical farms, SPF-14 are visited twice a day. Table 12 shows the breakdown

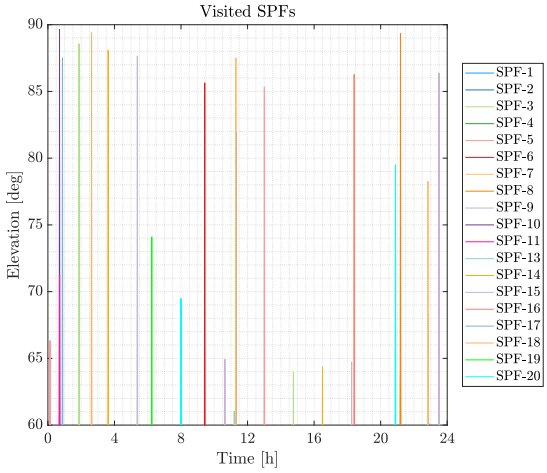

Fig. 15. Elevation profile of passes in the selected optimal Sun-synchronous orbit with SPFs included.

Table 11
Polar orbit pass sequence results.

SPF #	T_{pass} [min]	ϵ_{max} [deg]	E [MWh]
1	16.15	89.4	34.9
10	17.36	81.4	34.3
16	17.35	83.6	34.6
12	17.34	86.0	34.7
6	17.35	83.6	34.7
13	17.34	65.8	29.3
11	17.33	76.8	33.5
5	17.25	72.4	32.2
3	17.35	83.7	34.7
14	17.21	83.7	34.7
15	17.35	83.6	34.7
19	17.34	64.0	28.0
20	17.20	79.5	34.1
6	17.21	80.5	34.3
13	17.34	86.8	34.8
9	17.36	69.8	31.0
Total			534.4

of all passes with associated details on pass duration, elevation and quantity of energy delivered.

As mentioned, there are several near-overhead passes in the SSO case, which result in greater than 34 MWh energy delivered with the highest being 34.5 MWh. The total quantity of energy delivered per day is equal to 588.4 MWh. Compared to the polar orbit case in this subsection, the SSO provides approximately two additional near-overhead equivalent quantities of solar energy delivery. In comparison with the SSO case with the existing SPF in the previous subsection, the increase is approximately 62% (from 363.5 MWh to 588.4 MWh), again representing an approximately linear increase with the number of solar power farms (approx. 67%). Compared to Viale et al. [12], the quantity of energy delivered is more than doubled (from 283.4 MWh [12] to 588.4). It is also worth noting that, by increasing the number of solar power farms, the duty cycle of reflectors will also increase. The pass duration of a single reflector is 17.3 min on average. The total daily operation time with 18 passes would be approximately 5.2 h which

Table 12
SSO pass sequence results.

SPF #	T_{pass} [min]	ϵ_{max} [deg]	E [MWh]
5	16.15	66.3	29.2
10	17.36	89.6	34.4
3	17.35	88.6	34.3
18	17.34	89.4	34.5
14	17.35	88.1	34.4
15	17.34	87.6	34.4
19	17.33	74.0	32.8
20	17.25	69.5	30.5
6	17.35	85.6	34.3
9	17.21	64.9	28.5
7	17.35	87.5	34.4
5	17.34	85.3	34.3
3	17.20	63.9	27.9
14	17.21	64.4	28.1
16	17.34	86.3	34.3
8	17.36	89.3	34.4
7	17.32	78.3	33.4
9	17.36	86.4	34.3
Total			588.4

is approximately 21.6% of a day. By including several low-elevation passes, Viale et al. enhanced the duty cycle from approximately 5% to 15% with a total of 13 passes [12]. Therefore, even though the duty cycle in this paper has been increased only by 5% compared to Viale et al. [12], the energy delivered has been increased by more than 100% with additional and high-elevation passes. It is also noteworthy that the duty cycle in this paper is lower (13%) compared to Ref. [12] when existing farms are considered due to a smaller number of passes (11 in this paper vs. 13 in Ref. [12]). But ultimately the total quantity of energy delivered is higher due to higher elevation passes. Before further discussion, the results of optimisation can be summarised in Table 13.

Table 13
Summary of optimised orbits, number of distinct passes in a day and the quantity of energy delivered provided for existing and hypothetical SPF for comparison.

SPF	Case	Orbit	No. of passes	E_{tot} [MWh]
Existing (12)	Single	Polar	10	334
		SSO	11	363.5
	Two-reflector	Polar	17 (9 + 8)	564.5
		SSO	17 (7 + 10)	549.8
All (20)	Single	Polar	16	534.4
		SSO	18	588.4

The results in Table 13 could potentially be increased further with the optimisation of new SPF locations for a chosen orbit to ensure that hypothetical SPFs do not overlap with existing SPF or enable twice-daily passes. For the latter, for example, Fig. 14 shows favourable locations where groundtrack passes over the same location twice a day in North Africa or Australia, where some of the chosen hypothetical farms are located closely. Their location can be optimised in conjunction with orbit optimisation to achieve higher energy delivery. For example, if SPF-14 ([latitude, longitude] = [24.73 deg, 6.42 deg]) is located at a slightly higher latitude at the intersection point the quantity of energy delivered could be increased approximately by about 6.4 MWh per day. Similarly, if SPF-19 and SPF-20 are located favourably at the intersection, the total quantity of energy delivered to those farms could be approximately 138 MWh (34.5 MWh x 2 passes x 2 SPF) per day, instead of the current 63.3 MWh, or at least increase by 5.7 MWh to 69 MWh. Then, the total could reach approximately 600 MWh and could even increase to 635 MWh per day. Then the additional quantity of energy would be increased by approximately 75% (from 363.5 MWh to 635 MWh), higher than the increase in the number of SPF (67%) or approximately reach the same level at 65% (from 363.5 MWh to 600 MWh). The strategic placement of new solar power farms could also decrease the number of overlapping passes or increase the distinct passes, potentially increasing the energy delivery further. A final note can also be made for dawn/dusk reflectors, which demonstrated inferior performance per reflector on average. The reasoning was found to be the disproportionate distribution of SPFs in the eastern and western hemispheres of the Earth in this case. With the hypothetical farms, the ratio of the number of SPF between the eastern and western hemispheres increases from 0.33 (3 vs. 9) to 0.54 (7 vs. 13), which may improve the results of the dawn/dusk reflector case as well. Ultimately, however, orbiting reflector constellations will be aimed at increasing the quantity of energy delivered further.

Table 14
The results of extended pass duration and the quantity of energy delivered in different constellation options.

N	T_{pass} (mean) [min]	E_{tot} (existing) [MWh]	E_{tot} (hypothetical) [MWh]
5	34.5	1817.5	2942
10	56.0	3635	5884
20	98.9	7279	11 768

6. Constellations of orbiting solar reflectors

The results of a single orbit presented in the previous section can now be extended to a constellation. Here, a relatively small number of reflectors will be considered for a Sun-synchronous orbit constellation. Single reflectors will be considered for 5, 10 and 20 orbit planes and the results will be discussed for both existing and hypothetical SPF cases. Recall from Section 4 that the constellation orbits are circular and have the same orbital elements except for the right ascension of the ascending node, Ω. Also recall from the mathematical derivations in Section 3 that the appropriate selection of the RAAN difference between the orbit planes, $\Delta\Omega$ and mean anomaly ΔM between subsequent reflector orbits will provide the same pass geometry in terms of elevation. Hence the pass duration and the quantity of energy delivered would be scaled by the number of reflectors according to Eq. (10) for pass duration and linearly for the quantity of energy as $E_{tot} = NE$. The placement of orbit planes and the extension of pass duration requires a phase angle, ϕ, to be defined for the constellation. ϕ is selected to be 15 deg initially, but the implications of a smaller and a larger value will also be discussed later. According to this design choices, Table 14 summarises the constellation properties for the selected number of reflector satellites.

Table 14 shows that with just 5 reflectors, the extension of operations at a solar power farm would approximately be doubled and could be over 1.5 h with 20 reflectors. With 5, 10 and 20 reflectors and $\phi = 15\,\text{deg}$, the constellation would span a Ω range of 4.40, 9.90 and 20.9 deg. If the leading reflector is placed approximately at the terminator line, it would provide sufficient angular range before the Earth's shadow on the reflector occurs. The maximum allowable range extends up to approximately $\beta = 30.2\,\text{deg}$ from the terminator point for a 1000 km altitude orbit. The quantity of energy delivery linearly scales with the number of reflectors and reaches nearly 12 GWh for a 20-reflector constellation with the inclusion of hypothetical solar power farms. It is previously argued that if polar orbit RAAN is greater and smaller than 90 deg, there would be enhanced energy delivery at night due to the geometry with the Sun-line, according to Fig. 5. This is not true for SSOs, or at least the change is minuscule as previously demonstrated in a fully numerical model in Viale et al. [12], therefore the scalability would apply for the SSO case, as the similarity in different solutions in Table 7 also demonstrate. Then, Fig. 16 shows an example 10-reflector constellation with the reflectors' distribution in orbit.

The lead reflector satellite in Fig. 16 is the SSO solution in Table 10 with $\Delta\Omega$ and ΔM as given in Table 1 for $\phi = 15\,\text{deg}$. In the $y-z$

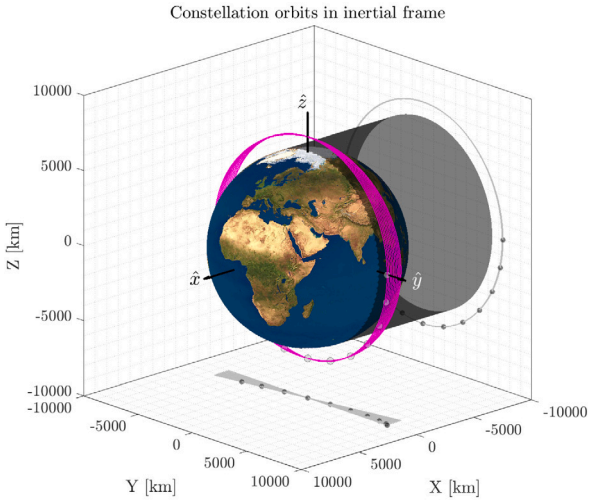

Fig. 16. Orbits and distribution of orbiting solar reflectors with 10 reflectors and ϕ = 15 deg phase angle between them. Each grey dot represents a reflector and magenta circles represent orbits.

projection of the orbits, the equal and $\phi = 15\,\text{deg}$ distribution can be seen.

It is also of interest how the profile of power delivered would appear with the separation between the reflectors. This has implications on the duration, intensity and uniformity of the power profile desired by the receiving solar power farm. The impact of the separation angle ϕ in this case will be discussed for a 10-reflector constellation and ϕ = 5, 15 and 30 deg. The assumption again is that the profiles are the same thanks to the favourable placement of reflectors in the constellation. Fig. 17 shows these combined power profiles together.

With the reflector constellation considered in Table 14, where $\phi = 15\,\text{deg}$, the power profile varies sinusoidally after the second reflector appears for approximately 40 min and the variation is bounded approximately between 380 and 550 MW. On the other hand, if ϕ is increased to 30 deg, the sinusoidal variation is between 60 to 490 MW, meaning that the overlap is not effective, but the advantage of larger ϕ is the extended pass duration of longer than 1.5 h. It is worth noting that if $\phi = 30\,\text{deg}$ or other larger numbers are selected, the Ω range may be greater than β angle for this altitude, therefore initial Ω needs to be smaller than 90 deg. Finally, if a smaller ϕ value is selected, such as $\phi = 5\,\text{deg}$ in Fig. 17a, then the power profile shows a much larger peak at 1400 MW, but the total pass duration decreases down to approximately 30 min.

The power profile could be adjusted according to the energy demand or other terrestrial or space segment requirements by modifying the orbit RAAN within the constellations. Changing the power profile from Fig. 17b to a, or $\phi = 15\,\text{deg}$ to 5 deg means that $\Delta\Omega$ and ΔM need to be reduced from 1.10 deg to 0.37 deg and from 14.98 deg to 4.99 deg, respectively. This may be achieved by solar radiation pressure by utilising the reflectors as solar sails. For a reflector of areal density of 18.8 gm^{-2} in a circular orbit similar to this paper (at 884.6 km), the authors found that 1 deg shift in Ω may be achieved in approximately 10 days, if the reflector is Sun facing. The change in Ω is smaller here (approximately 0.7 deg), therefore a faster change may be expected.

Alternatively, the sinusoidal variations in Fig. 17b and c can be made more uniform by using a large number of smaller reflectors with smaller spacing between them. To demonstrate this, the power profile in Fig. 17b will be considered. To that end, the area of a single 1 km diameter reflector is equal to 25 200-m diameter reflectors. Then, as the equivalent of a 10-reflector constellation, there would be 250 reflectors with a 200-m diameter each. Dividing the Ω range for this constellation into 250 equal angles and converting them into ϕ through Eqs. (20) and (17) result in a spacing of $\phi = 0.5413\,\text{deg}$ between the reflectors. Combining the power profiles of the smaller reflectors would result in the power profile in Fig. 18.

Fig. 18 shows a square wave like, uniform power delivery profile. This provides approximately 445 MW power for approximately 40 min of nearly an hour pass duration. A similar approach may also be taken when $\phi = 30\,\text{deg}$, but in that case, the uniform maximum power delivered would be lower, but delivered in a longer duration. Using smaller reflectors in this form in a constellation may provide several advantages. First, it may be preferable from the solar power farm operation perspective where the reflectors provide uniform constant power delivery for an apriori known duration. Second, it may be preferable from a space segment perspective, as smaller reflectors have more manageable attitude control requirements [12] and may be easier to build and launch than single monolithic reflectors of 1 km in diameter.

Some final remarks could also be made about the potential contribution of orbiting solar reflector constellations to terrestrial electricity generation. Energy generation can be quantified by the capacity factor, which defines the ratio between the total electricity generated by that source and the total capacity for a given time. Utility-scale solar power farms currently have a global average capacity factor of approximately 0.17,[2] i.e., a solar power farm would generate electricity approximately 17% of its nameplate capacity over a year. As a reference, the global average capacity factor is approximately 0.4 for wind and more than 0.9 for nuclear energy in 2011-2013 [26]. The greatest inhibitor of the capacity factor for solar energy is the daylight limitation.

The US average capacity factor is 0.25 in 2014-2017 [27], which means that, for example, the 550 MW capacity Topaz solar power farm (SPF-11 in Table 2) would generate approximately 3300 MWh electricity per day on average. A 10-reflector constellation would deliver 3635 MWh solar energy to existing SPFs globally, from which, approximately 363.5 MWh electricity can be generated with a 20% conversion and 50% land-coverage ratios, i.e., approximately equivalent to 11% of the actual daily capacity of Topaz. The number can be doubled for a 20-reflector constellation, providing an approximately 22% increase and can be approximately linearly scaled. If hypothetical solar power farms are included in this comparison, then a 20-reflector constellation could generate electricity equivalent to 36% of Topaz capacity with 1176.8 MWh. If looked at globally, existing SPF capacity (except for SPF-12, which is not yet operational) may be linearly scaled to that of a 10-km diameter circular SPF area (i.e., approximately 78.5 km) for a comparison. The SPF with a larger area than $78.5\,\text{km}^2$ is not scaled down but instead kept constant. Again, with a global average capacity factor assumption of 0.17, the electricity generated in the existing SPF is approximately equal to 181.02 GWh per day. A 20-reflector constellation would then enhance the electricity generation by about 0.4% globally with 728 MWh, at potentially a fraction of the cost of all 11 SPFs combined [12]. Further enhancement can be achieved by increasing the number of reflectors in the constellation. Orbiting solar reflector constellations may then be seen as analogous to additional solar power farms in space, that provide near-constant daily solar energy delivery, i.e., a near-constant capacity factor throughout the year, enhancing the existing terrestrial solar energy globally.

7. Conclusions

Constellations of orbiting solar reflectors could enhance terrestrial solar energy generation by providing additional illumination to solar power farms on Earth. This specific application requires constellation reflectors to be placed near the dawn/dusk terminator region and to follow a similar pass geometry for continuous, predictable and scalable

[2] Available at https://www.statista.com/statistics/799330/global-solar-pv-installation-cost-per-kilowatt/, Accessed August 29, 2023.

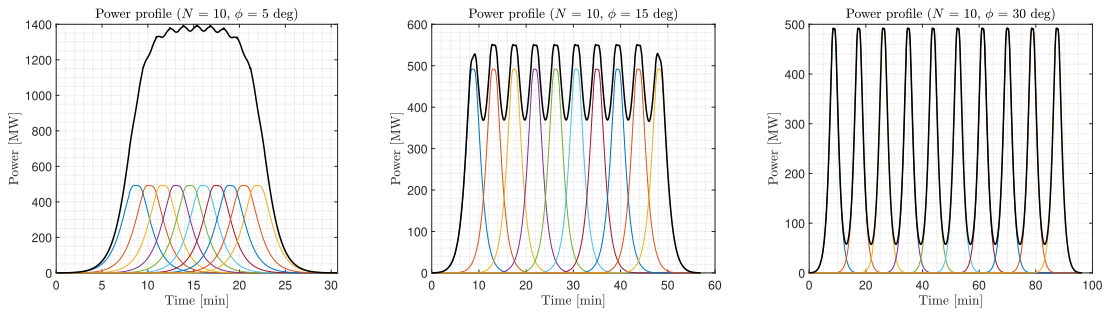

(a) $\phi = 5\,\text{deg}$ (b) $\phi = 15\,\text{deg}$ (c) $\phi = 30\,\text{deg}$

Fig. 17. Combined power profile of a 10-reflector constellation with phase angles 5, 15, 30 deg between the reflectors. Individual power profiles are shown with coloured figures. (For interpretation of the references to colour in this figure legend, the reader is referred to the web version of this article.)

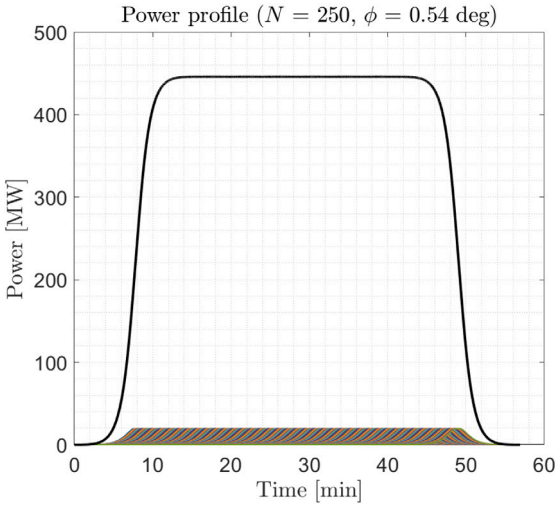

Fig. 18. Power profile of 250 200-m diameter reflectors in a constellation adopted from 10-reflector constellation with $\phi = 15$ deg. Individual profiles are shown with coloured figures.

solar energy delivery. This paper therefore investigates constellations that address these requirements and analyses their properties.

First, the equations of Walker-type constellations are modified in the presence of the Earth's oblateness perturbation such that successive reflectors repeat the same elevation profile over solar power farms. Such a formulation also allows for optimising only one orbit's groundtrack and extrapolating its properties to the other reflectors in the constellation. Using this favourable property, the genetic optimisation of groundtracks of circular polar and Sun-synchronous orbits (SSO) is performed with an objective function defined as the total quantity of energy delivered to predefined solar power farms on the Earth. The optimisation is performed for either a single reflector per orbit or two-reflector (placed 180 deg apart) per orbit. Among all cases, SSO and single reflector cases were found to be superior. A constellation with 20 reflectors could deliver a significant quantity of solar energy to existing solar power farm projects, which may be enhanced even further with strategically placed new solar power farms. Constellations of orbiting solar reflectors could then be seen as analogous to additional solar power farm in space, distributing solar energy globally rather than locally, enhancing the capacity of terrestrial solar energy.

This paper has only considered a single orbit altitude and a limited set of possible orbital configurations, which, nevertheless, has demonstrated the potential of solar reflector constellations to enhance terrestrial solar energy generation. Alternative constellation geometries could enhance this further for a truly global clean energy generation by orbiting solar reflectors.

Declaration of competing interest

The authors declare that they have no known competing financial interests or personal relationships that could have appeared to influence the work reported in this paper.

Acknowledgements

This project has received funding from the European Research Council (ERC) under the European Union's Horizon 2020 research and innovation programme (grant agreement No. 883730). CRM is also supported by the Department of Science, Innovation and Technology (DSIT) and the Royal Academy of Engineering under the Chair in Emerging Technologies programme, United Kingdom. For the purpose of open access, the author(s) has applied a Creative Commons Attribution (CC-BY) licence to any Author Accepted Manuscript version arising from this submission.

References

[1] H. Oberth, Methods of Space Travel, Munich, Oldenburg, 1929, p. 494.
[2] K.W. Billman, W.P. Gilbreath, S.W. Bowen, Introductory Assessment of Orbiting Reflections for Terrestrial Power Generation, Tech. Rep. NASA-TM-73230, National Aeronautics and Space Administration, Scientific and Technical Information Branch, NASA, 1977.
[3] K.A. Ehricke, Space light: space industrial enhancement of the solar option, Acta Astronaut. 6 (12) (1979) 1515–1633, http://dx.doi.org/10.1016/0094-5765(79)90003-1.
[4] J.E. Canady, J.L. Allen, Illumination from Space with Orbiting Solar-Reflector Spacecraft, Tech. Rep. NASA-TP-2065, National Aeronautics and Space Administration, Scientific and Technical Information Branch, NASA, 1982.
[5] O. Çelik, A. Viale, T. Oderinwale, L. Sulbhewar, C.R. McInnes, Enhancing terrestrial solar power using orbiting solar reflectors, Acta Astronaut. 195 (2022) 276–286, http://dx.doi.org/10.1016/j.actaastro.2022.03.015.
[6] L.M. Fraas, Mirrors in space for low-cost terrestrial solar electric power at night, in: 38th IEEE Photovoltaic Specialists Conference, IEEE, Austin, TX, 2012, pp. 2862–2867, http://dx.doi.org/10.1109/PVSC.2012.6318186.
[7] L.M. Fraas, G.A. Landis, A. Palisoc, Mirror satellites in polar orbit beaming sunlight to terrestrial solar fields at dawn and dusk, in: 2013 IEEE 39th Photovoltaic Specialists Conference, PVSC, IEEE, Tampa, FL, 2013, pp. 2764–2769, http://dx.doi.org/10.1109/PVSC.2013.6745046.
[8] L. Fraas, G.A. Landis, A. Palisoc, P. Jaffe, Space solar power, mirror development and the international space station, in: 67th International Astronautical Congress, IAC2016, IAF, Guadajalara, Mexico, 2016, Paper no. IAC-16-C3.4.3x32179.
[9] L.M. Fraas, M.J. O'Neill, Sunbeams from space mirrors for terrestrial PV, in: Low-Cost Solar Electric Power, Springer International Publishing, Cham, ISBN: 978-3-031-30812-3, 2023, pp. 163–176, http://dx.doi.org/10.1007/978-3-031-30812-3_12.
[10] L. Fraas, Space mirror orbit for municipal street lighting, in: 70st International Astronautical Congress, IAC 2019, IAF, Washington, DC, USA, 2019, Paper no. IAC-19, C3, 1, 5, x49543.
[11] F. Bonetti, C. McInnes, Space-enhanced terrestrial solar power for equatorial regions, J. Spacecr. Rockets 56 (1) (2019) 33–43, http://dx.doi.org/10.2514/1.A34032.

[12] A. Viale, O. Çelik, T. Oderinwale, L. Sulbhewar, C.R. McInnes, A reference architecture for orbiting solar reflectors to enhance terrestrial solar power plant output, Adv. Space Res. 72 (4) (2023) 1304–1348, http://dx.doi.org/10.1016/j.asr.2023.05.037.

[13] A. Viale, O. Çelik, T. Oderinwale, L. Sulbhewar, G. Bailet, C.R. McInnes, Towards the commercial development of orbiting reflectors: a technology demonstration roadmap, in: 73rd International Astronautical Congress, IAC 2022, IAF, Paris, France, 2022, Paper no. IAC–22–C3.2.x70070.

[14] O. Çelik, C.R. McInnes, Families of displaced non-Keplerian polar orbits for space-based solar energy applications, in: 73rd International Astronautical Congress, IAC 2022, IAF, Paris, France, 2022, Paper no. IAC-22-C1.IP.37.x69012.

[15] T. Oderinwale, C.R. McInnes, Enhancing solar energy generation and usage: Orbiting solar reflectors as alternative to energy storage, Appl. Energy 317 (2022) 119154, http://dx.doi.org/10.1016/j.apenergy.2022.119154.

[16] O. Çelik, C.R. McInnes, An analytical model for solar energy reflected from space with selected applications, Adv. Space Res. 69 (1) (2022) 647–663, http://dx.doi.org/10.1016/j.asr.2021.10.033.

[17] D. Mortari, M.P. Wilkins, C. Bruccoleri, The flower constellations, J. Astronaut. Sci. 52 (2004) 107–127, http://dx.doi.org/10.1007/BF03546424.

[18] J.G. Walker, Satellite constellations, J. Br. Interplanet. Soc. 37 (1984) 559.

[19] D. Arnas, D. Casanova, Nominal definition of satellite constellations under the earth gravitational potential, Celestial Mech. Dynam. Astronom. 132 (2020) 1–20, http://dx.doi.org/10.1007/s10569-020-09958-4.

[20] O. Çelik, C.R. McInnes, A generic three-dimensional model for solar energy reflected from mirrors in circular orbits, Adv. Space Res. 72 (11) (2023) 5047–5069, http://dx.doi.org/10.1016/j.asr.2023.09.046.

[21] H.C. Hottel, A simple model for estimating the transmittance of direct solar radiation through clear atmospheres, Solar Energy 18 (2) (1976) 129–134, http://dx.doi.org/10.1016/0038-092X(76)90045-1.

[22] I. Moore, L. Sulbhewar, O. Çelik, C.R. McInnes, The effects of pointing error sources on energy delivery from orbiting solar reflectors, in: 74th International Astronautical Congress, IAC 2023, IAF, Baku, Azerbaijan, 2023, Paper no. IAC-23, C1, 1, 6, x76505.

[23] H. Yi, W. Lei, F. Wenju, Z. Haitao, L. Tao, X. Beizhen, C. Ruizhi, LEO navigation augmentation constellation design with the multi-objective optimization approaches, Chin. J. Aeronaut. 34 (4) (2021) 265–278, http://dx.doi.org/10.1016/j.cja.2020.09.005.

[24] V.A. Chobotov, Orbital Mechanics, AIAA, 2002, pp. 415–416, http://dx.doi.org/10.2514/4.862250.

[25] D.E. Goldberg, Genetic Algorithms in Search, Optimization and Machine Learning, Addison-Wesley Longman Publishing Co., Inc., 1989.

[26] US Energy Information Administration, Monthly generator capacity factor data now available by fuel and technology, 2014, https://www.eia.gov/todayinenergy/detail.php?id=14611. Accessed September 8, 2023.

[27] US Energy Information Administration, Southwestern states have better solar resources and higher solar PV capacity factors, 2019, https://www.eia.gov/todayinenergy/detail.php?id=39832#:~:text=On%20average%2C%20utility%2Dscale%20solar,values%20from%202014%20through%202017. Accessed August 29, 2023.